
MONET: A Massive, Open, Non-redundant and Enriched Text-to-image dataset

Benjamin Aubin*
Jasper Research

Gonzalo Iñaki Quintana
Jasper Research

Onur Tasar
Jasper Research

Sanjeev Sreetharan
Jasper Research

Urszula Czerwinska
Jasper Research

Damien Henry
Jasper Research

Clément Chadebec*
Jasper Research

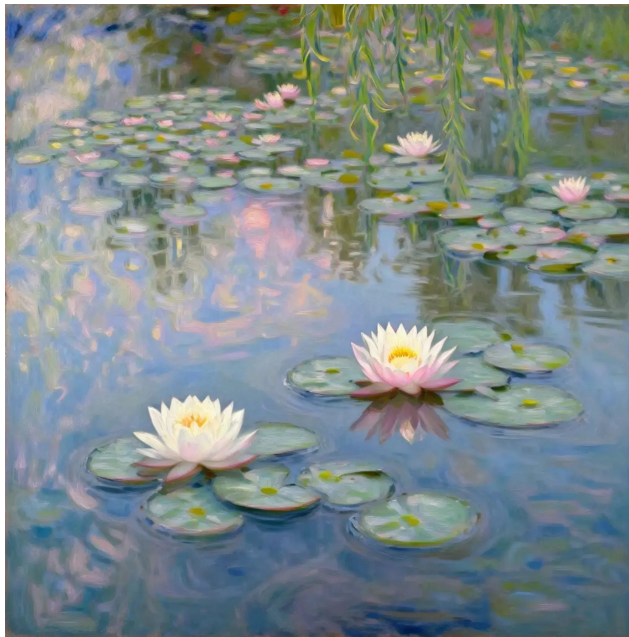


Figure 1: An impressionist water-lily painting generated at 2048×2048 by our 4B text-to-image model trained *exclusively* on the MONET dataset, in homage to Claude Monet’s *Nymphéas* series.

Abstract

Training large text-to-image models requires high-quality, curated datasets with diverse content and detailed captions. Yet the cost and complexity of collecting, filtering, deduplicating, and re-captioning such corpora at scale hinders open and reproducible research in the field. We introduce MONET, an open *Apache 2.0* dataset of ~ 104.9 M image–text pairs collected from 2.9B raw pairs across heterogeneous open sources through successive stages of safety filtering, domain-based filtering, exact and near-duplicate removal, and re-captioning with multiple vision-language models covering short to long-form descriptions, and further augmented with synthetically generated samples. Each image is shipped with pre-computed embeddings and annotations to accelerate downstream use. To validate the effectiveness of MONET, we train a 4B-parameter latent diffusion model *exclusively* on it and reach competitive GenEval and DPG scores, demonstrating that our dataset lowers the barrier to large-scale, reproducible text-to-image research.

*Corresponding authors: surname.name@jasper.ai

1 Introduction

Text-to-image (T2I) models have shown remarkable progress in generating realistic images from text descriptions [72, 73, 33, 78, 76, 68, 44, 10, 11, 19]. However, training such models requires large, curated corpora with strong visual diversity, high-quality images, and detailed captions. Collecting, filtering, deduplicating, and re-captioning such datasets at scale is expensive and time-consuming, restricting state-of-the-art T2I research to a handful of well-resourced players and hindering open, transparent, and reproducible work in the field. Early open initiatives, such as YFCC100M [90], LAION-400M / LAION-5B [81, 82], and COYO-700M [6], have provided hundreds of millions to billions of web-crawled image–text pairs, but remain largely uncurated, highly redundant, and paired with short, noisy alt-text captions.

Recent works have shown that richer captions significantly boost T2I performance [3, 10, 19], motivating the creation of synthetically re-captioned datasets such as ShareGPT4V [13] (1.2M images). However, this dataset remains too small for pre-training large T2I models, and relying on a single Vision-Language Model (VLM) tends to bias the caption distribution and degrade out-of-distribution generation [19, 97]. To the best of our knowledge, no **openly released, filtered, deduplicated, and multi-VLM re-captioned** dataset is currently available for pre-training T2I models at scale.

In this paper, we bridge this gap by introducing **MONET**, a new large-scale dataset of **104.9M** image–text pairs released under the permissive *Apache2.0* license and specifically designed for training large T2I models. The dataset is available at <https://huggingface.co/datasets/jasperai/monet/>. MONET is distilled from 2.9B raw pairs collected across nine heterogeneous open sources (6 *real* and 3 *synthetic*), using aesthetic pre-filtering, multi-classifier safety filtering, deduplication, and domain-based filtering for source governance. Each surviving image is re-captioned by multiple VLMs, ranging from short concept-level to long fine-grained descriptions, and the corpus is augmented with synthetic samples generated by *Apache 2.0* T2I models. All samples are shipped with standard image embeddings (DINOv2 [64], CLIP [70], SSCD [66]), classifiers and detectors (YOLO [41], Mediapipe [61]), and pre-encoded with SANA VAE [102]. We also provide a comprehensive analysis of the dataset, including statistics, content and topic analyzes, and human quality assessment, and validate its usefulness by training a 4B-parameter T2I model exclusively on MONET, which achieves competitive evaluation scores.

2 Related work

Text-to-image models Although early GAN-based approaches [27, 104, 79, 44] laid the groundwork for text-conditioned image generation, diffusion [84, 32, 86] and flow-based models [60, 58] have become the dominant paradigms for T2I synthesis [72, 73, 33, 78, 76, 74, 68, 10, 11, 19, 101, 97, 102]. These methods pair a powerful text encoder, whose output serves as a conditioning, with a denoiser instantiated as a U-Net [77] or transformer [93, 65]. More recently, the success of Large Language Models (LLMs) [4, 34, 28, 89, 59, 40] has motivated unified architectures that process all modalities in a shared space, either through autoregressive next-token prediction [96, 88, 14, 98, 99], hybrid prediction–diffusion schemes [109, 111, 62, 103], or discrete diffusion [87, 55].

Text–image datasets Progress in VLMs and T2I models has been driven by the availability of large-scale image–text datasets. Early curated datasets such as MS-COCO [57], Visual Genome [47], and Conceptual Captions (CC3M, CC12M) [83, 9] provide filtered image–text pairs useful for training captioning models, but their scale remains limited to several hundred thousand or several million samples, capping model scalability. Subsequent web-scale efforts [36, 39, 17] relied on noisy alt-text or social-media captions to reach hundreds of millions of pairs, culminating in YFCC100M [90], LAION-400M / LAION-5B [81, 82] and COYO-700M [6]. Although these corpora enabled foundational VLMs and T2I models such as CLIP [70] and Stable Diffusion [76], they remain highly redundant and contain misaligned, unfiltered, or unsafe content – issues partially addressed by the safety-revised Re-LAION [50]. To improve caption quality, several works re-caption images with VLMs [3, 10, 19], most notably ShareGPT4V [13], which provides 1.2M GPT-4V-generated captions but is too small for large-scale pre-training and tied to a single captioner, biasing the dataset toward a single prompt distribution.

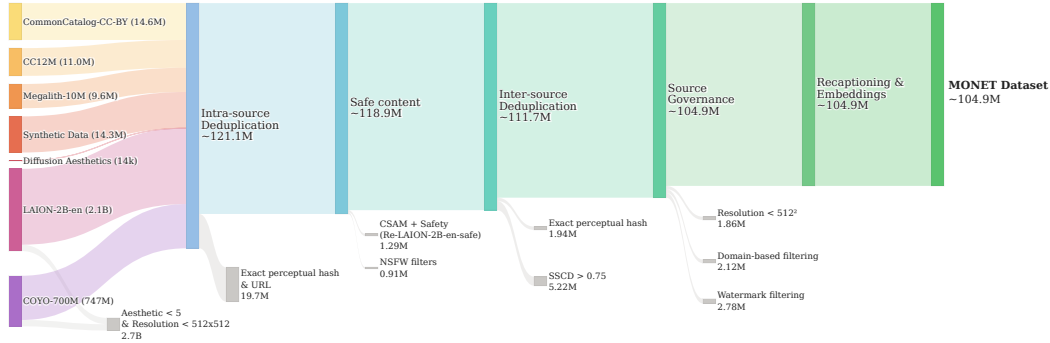


Figure 2: Curation pipeline of the MONET. Each stage removes images that fail the corresponding quality, safety or source-governance checks, while the surviving pool flows to the next step.

Dataset curation Data quality is now widely accepted to matter more than raw quantity for training large multimodal models [110, 10, 69, 19], since uncurated web data is noisy and often misaligned. Early curation pipelines relied on simple aesthetic scores [51] or CLIP-score [70] thresholding to enforce image–text alignment. More recent efforts, such as the DataComp benchmark [22], systematically search the filter-design space, while Data Filtering Networks [20] train specialized models to score and discard low-quality or misaligned samples. MONET builds upon these curation strategies by combining rigorous aesthetic, safety, and watermark filtering with pre-trained network models and careful re-captioning using various captioning models of varying complexity, thereby enabling a rich and diverse prompt distribution.

Data deduplication An often under-addressed issue in large multimodal corpora is the prevalence of duplicate or near-duplicate samples, which skew the data distribution and induce memorization [43, 52], a particularly pressing concern for diffusion models [85, 8]. MONET addresses this issue by using a combination of deduplication methods, such as perceptual hashing [94] and Self-Supervised Copy Detection (SSCD) [66], to remove near-duplicate images from the dataset.

3 Dataset construction

In this section, we detail the construction of the MONET dataset. Starting from heterogeneous open sources totaling 2.9B raw image–text pairs, we apply successive stages of pre-filtering, safety filtering, deduplication, and domain-based filtering, followed by multi-VLM re-captioning and synthetic-data augmentation, to obtain a final dataset of **104.9M** high-quality and safe image–text pairs. The complete curation pipeline is illustrated in Fig. 2.

3.1 Data sourcing

MONET is built from existing open-source datasets selected via source-governance criteria, chosen to maximize diversity in content, visual style, and resolution while supporting reproducibility. As summarized in Table 1, the bulk of the pool (>2.8B images, from LAION, COYO and CC12M) comes with noisy *alt-text* captions, while 14.6M images are pre-captioned with VLMs such as BLIP2 [54] (Common-Catalog) and 14k with GPT-4o [38] (Diffusion-Aesthetic-4K). Finally, 9.6M images have no captions (Megalith-10M). We deliberately exclude several popular alternatives relying on Common Crawl, such as DataComp-1B [22], since they heavily overlap with LAION and COYO, as well as the non-English part of LAION-5B [82], since multilingual coverage is more reliably obtained via translation than from noisy *alt-text*.

3.2 Pre-filtering

For the two largest sources, LAION and COYO, we apply two pre-filters before merging them with the smaller datasets, concentrating computational resources on images that meet our baseline quality requirements. First, we exclude images with a resolution below 512^2 pixels, as low-resolution samples typically lack sufficient detail, reducing the effectiveness of pretraining. Second, we filter

Table 1: Summary of the sources used in compiling MONET, together with approximate statistics and licensing information. Top rows correspond to real image–text sources, while bottom rows report images generated synthetically (see Sec. 3.7).

Dataset Name	# Images (original)	# Images (final)	Image source	Caption source	License
LAION (2B-en) [81]	2.1B	46.6M	Common Crawl	Alt-text	CC-BY-4.0
COYO [6]	747M	19.1M	Common Crawl	Alt-text	CC-BY-4.0
Common-Catalog-CC-BY [26]	14.6M	11.2M	Flickr*	BLIP2	CC-BY-4.0
Megalith-10M	9.6M	8.0M	Flickr	None	MIT (metadata)
Conceptual-12M [9]	11.0M	6.4M	Web	Alt-text	Google (Permissive)
Diffusion-Aesthetic-4K [108]	14k	12.8k	Web	GPT-4o	MIT
<i>Synthetic data (see Sec. 3.7)</i>					
Z-Image [106]	6.2M	5.9M	Synthetic	Synthetic	Apache 2.0
FLUX.2-klein-4B [49]	3.6M	3.5M	Synthetic	Synthetic	Apache 2.0
FLUX.1-schnell [48]	4.5M	4.4M	Synthetic	Synthetic	Apache 2.0

* Images extracted from YFCC100M [90]

out images with an aesthetic score [51] below 5.0, shifting the pool toward more visually appealing samples (see Fig. 3). Combined, these two filters retain roughly 91M images from LAION and COYO. After merging with the four smaller real-image sources and applying intra-source URL/pHash deduplication (described in Sec. 3.4), we obtain a **121.1M** merged pool that serves as the reference baseline for the cumulative reductions reported in the remaining stages.



Figure 3: Examples of images at different aesthetic scores [51]. A lower aesthetic score is correlated with lower-quality or visually unappealing images, motivating the pre-filtering stage.

3.3 Safety filtering

Since the data come mainly from the Web, we apply strict safety filters to the merged pool. We start by restricting LAION-2B-en samples to those also present in the vetted Re-LAION-2B-en-safe release [50], removing 1.29M images flagged during the Re-LAION safety revision. Second, we apply an ensemble of open-source *Not-Safe-For-Work* (NSFW) detectors (Falcon [1] and Bumble [5]) together with an internal classifier, under a conservative union rule: an image is removed if any classifier flags it. This leverages the complementary failure modes of the detectors to minimize false negatives at the cost of some false positives, and removes an additional 0.91M images. Finally, we conduct a safety audit using DINOv2 [64] embeddings by manually inspecting the 100 nearest neighbors of a small seed set of NSFW images; no additional harmful content is detected, thereby supporting the effectiveness of the previous steps. After safety filtering, the pool is reduced to **118.9M** safe images (1.8% cumulative reduction). While no filtering pipeline can guarantee perfect coverage, this multi-layered approach substantially reduces the likelihood that harmful content will persist in the final dataset. See Appendix A.1 for more in-depth discussion on the filters used.

3.4 Deduplication

Deduplication is crucial to ensure diversity and prevent memorization and overfitting [52, 43, 85, 29]. We use a two-stage strategy combining exact and near-duplicate detection.

URL and perceptual hashing We start by removing exact URL duplicates, then apply DCT-based perceptual hashing (pHash) [94] to detect near-exact copies that differ only in compression or scaling. These steps are applied first to each source individually (removing ~ 19.7 M intra-source duplicates) and then to the merged safe pool (removing 1.94M additional inter-source duplicates). Because pHash retains only the lowest-frequency DCT coefficients, it cannot capture geometric transforms such as flips, crops, or color shifts and is therefore unreliable for identifying near-duplicates: such

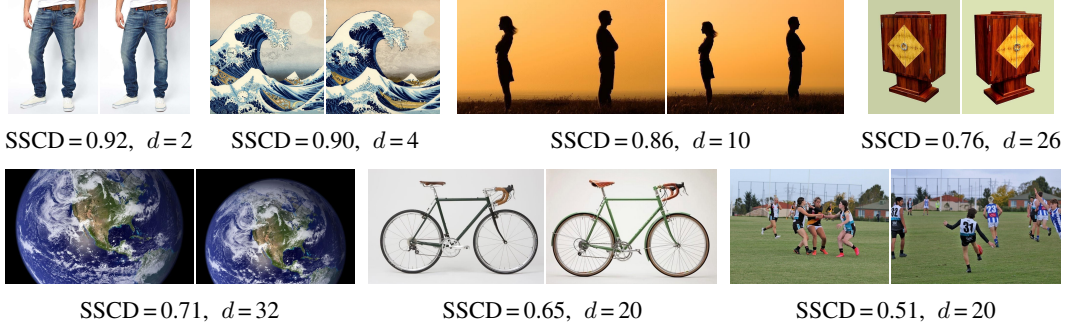


Figure 4: SSSD nearest-neighbor pairs with cosine similarity and pHash Hamming distance d . *Top*: near-duplicates removed ($\text{SSCD} \geq 0.75$); pHash degrades under flips, crops, or background swaps while SSSD remains high. *Bottom*: semantic neighbors retained ($\text{SSCD} < 0.75$).

pairs can reach large Hamming distances, overlapping the range of unrelated images and precluding a reliable threshold (see Fig. 4).

SSCD near-duplicate detection To handle near-duplicates, we rely on Self-Supervised Copy Detection (SSCD) [66]. We compute 512-d SSCD embeddings with the public `sscd_disc_mixup` model [67] and retrieve the $k = 64$ nearest neighbors per image using a FAISS index [18]; $k = 64$ trades off search speed against cluster recall, and is large enough to cover the maximum near-duplicate cluster size we observe empirically. Pairs whose cosine similarity exceeds 0.75 are collapsed (keeping the representative with the highest resolution and aesthetic score) removing 5.22M additional images. The 0.75 threshold corresponds to the operating point recommended by the SSCD authors at 90% precision on DISC [67], and we validate it on our data by manually inspecting pair slices at 0.05 resolution (see Fig. 4). We find that pairs above 0.75 are consistently near-duplicates (crops, flips, color shifts, watermarks), while pairs below 0.75 are semantically related but visually distinct (*e.g.* different frames from the same series), which we retain for diversity. After deduplication, the pool contains **111.7M** unique images (7.7% cumulative reduction). See Appendix A.2 for more details and limitations about the deduplication strategy.

3.5 Domain-based filtering and source governance

A final round of exclusion-based filters enforces resolution, source, and watermark standards. We remove images with resolution below 512^2 pixels (1.86M images, mostly from the smaller sources, which were not pre-filtered in Sec. 3.2); then images originating from a blacklist of domains including known stock-photo providers such as *dreamstime*, *shutterstock*, *freepik*, *getty*, *unsplash*, etc. (2.12M images); and finally images flagged with high watermark probability by an internal detector (2.78M images) are discarded, leaving a final pool of **104.9M** images (13.4% cumulative reduction). These exclusion controls are not a representation of legal clearance; they are source-governance signals that reduce the prevalence of images from known restrictive providers.

3.6 Re-captioning

Caption quality and diversity are both crucial for T2I models. Recent works have shown that richer captions significantly boost model performance [3, 10, 19, 69], but human-annotated captions are prohibitively expensive at the scale of hundreds of millions of images. A widely adopted alternative is to synthesize image captions using pre-trained vision-language models [38, 13]. However, relying on a single captioner biases the prompt distribution and can degrade out-of-distribution generation [19, 97]. To mitigate this, we re-caption MONET with multiple VLMs of varying complexity. We first benchmark several candidates: BLIP2 [54], Florence2 [100], FastVLM [92], CogVLM1/2 [95, 35], InternVL3-8B/14B/38B [112], GPT-4V via ShareGPT4V-style captioning [13] and Gemini-2.5-flash-lite [15]; and compare caption complexity, latency and quality on 100 diverse images. Based on these trade-offs, we retain only Florence2-Large, InternVL3-8B, ShareGPT4V-7B, and Gemini-2.5-flash-lite. Florence2-Large produces short, concept-level captions that closely match typical user prompts, while the three remaining models yield long, fine-grained descriptions. A representative example

is shown in Fig. 6; additional examples are provided in Appendix A.3. To validate this selection, we correlate automatic alignment scores with ELO scores from human voting. We observe that the standard CLIP metric correlates poorly with human judgment on long captions since its 77-token context truncates most detailed outputs. We therefore report alignment with LongCLIP [107] in Fig. 7a, which handles longer inputs and tracks human preferences more faithfully. The conclusion holds for other long-context encoders such as Jina-CLIP-v2 [46], see Appendix A.3.2. Representative re-captioning examples, CLIP/LongCLIP alignment scores, ELO correlations, and the human-voting methodology are reported in Appendix A.3.

3.7 Synthetic data

We complement real data with synthetic images generated by FLUX.1-schnell [48], FLUX.2-klein-4B [49], and Z-Image [106], chosen as top-performing T2I models released under the permissive *Apache 2.0* license, which allows redistribution and use of their outputs for training. Prompts are drawn from recaptioning (Sec. 3.6) and an open-source prompt collection [42], then upsampled with Qwen3-4B [105] under a system prompt that removes unsafe content. The generated images are filtered with the same NSFW and watermark detectors used in Sec. 3.3 and the domain-based filters of Sec. 3.5. Examples are shown in Fig. 5. As shown in Sec. 5.2, mixing in moderate amounts of synthetic data improves text–image alignment.



Figure 5: Examples of synthetic images generated for the MONET dataset using different models. Prompts are drawn from MONET and [42], then upsampled with Qwen3-4B [105].

3.8 Image encoding & VAE pre-encoding

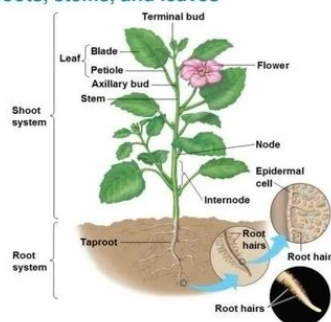
To accelerate downstream use, each MONET image is shipped with pre-computed embeddings, structured annotations, and latents, avoiding repeated raw-pixel processing. We store three complementary image embeddings: DINOv2-vitg14 [64] for general-purpose scene representations (retrieval, classification), CLIP-vit-base-patch32 [70] for image–text alignment (cross-modal search, zero-shot classification), and SSCD [66] supporting vector search, and deduplication at scale. We release the FAISS indexes for all the embeddings at <https://huggingface.co/spaces/jasperai/monet-retrieval>. We further release compact annotations from lightweight models, directly usable for filtering, balancing, and conditional generation: YOLO-v9e object detection [75, 41] (80 COCO categories, for object-centric queries and layout-conditioned generation), YOLO-v8x image classification [41] (distribution over 1,000 ImageNet-1k categories), and MediaPipe face detection [61] (face counts, boxes, and landmarks, for portrait filtering and privacy-aware subsampling). Finally, each image is accompanied by a pre-encoded latent from the SANA VAE [102], enabling latent diffusion training directly on compressed representations and cutting storage, bandwidth, and encoding time.

3.9 Computational cost of the dataset

Constructing MONET required $\sim 175\text{k}$ GPU-hours on a cluster of 60 L40S and 80 H200 GPUs, dominated by re-captioning ($\sim 79\%$), followed by domain-based filtering ($\sim 14\%$), and deduplication, synthetic generation, and feature / VAE pre-encoding ($\sim 2\text{--}3\%$ each). The end-to-end pipeline took several months of wall-clock time. By releasing MONET together with its multi-VLM captions, embeddings, annotations, and pre-computed VAE latents, we aim to substantially lower the barrier to reproducible text-to-image research at scale.

Re-captioning example

31.3 A typical plant body contains three basic organs: roots, stems, and leaves



Original: 31.3 A typical plant body contains three basic organs: roots, stems, and leaves

Florence: The image shows a plant with a flower, its roots, stems, and leaves clearly visible. The poster also contains text, providing further information about the plant's anatomy.

ShareGPT4V: The image presents a detailed diagram of a plant's anatomy, focusing on the root system. The plant is depicted with a pink flower at the top, surrounded by green leaves. The root system is shown in a cross-section view, revealing the taproot and root hairs. The diagram is labeled with the names of the different parts, such as the shoot system, leaf, stem, terminal bud, flower, node, intermodal cell, and root hairs. The diagram is a visual representation of the plant's structure, providing a clear understanding of its anatomy.

Gemini 2.5 Flash Lite: The image is a detailed illustration of a typical plant's basic organs: roots, stems, and leaves, accompanied by magnified views of root hairs and epidermal cells. The main object is a vibrant green plant with a pink flower blooming from its upper portion. The plant is divided into two main systems: the shoot system, which includes the leaves, stem, axillary bud, terminal bud, and flower; and the root system, which consists of a taproot and numerous root hairs extending into the soil. The scene depicts the plant partially submerged in brown soil, with the shoot system above ground and the root system below. Various parts of the plant are labeled with text, such as "Leaf" (further broken down into "Blade" and "Petiole"), "Stem", "Flower", "Terminal bud", "Axillary bud", "Node", and "Internode". Two inset circles provide magnified views: one shows the internal structure of a root, highlighting "Root hairs" emerging from epidermal cells, and the other provides a close-up of these fine, hair-like structures. The style is educational and illustrative, using clear lines, vibrant colors, and informative labels to convey botanical information effectively. The caption at the top, "31.3 A typical plant body contains three basic organs: roots, stems, and leaves," sets the context for the diagram.

InternVL3-8B: The image illustrates the structure of a typical plant body, emphasizing its three fundamental parts: roots, stems, and leaves. The root system is depicted beneath the soil, showcasing the taproot along with numerous root hairs that facilitate water absorption. The shoot system is illustrated vertically, highlighting nodes, internodes, and buds, including the axillary bud and terminal bud. Leaves, attached to the stem via petioles, are also detailed, showing the blade and flower structures. The image indicates that the root hair cell is not the same as the epidermal cell.

Figure 6: Representative re-captioning example, comparing the **original** web caption with captions produced by **Florence2**, **ShareGPT4V**, **Gemini 2.5 Flash Lite** and **InternVL3-8B**. Additional examples are reported in Appendix A.3.

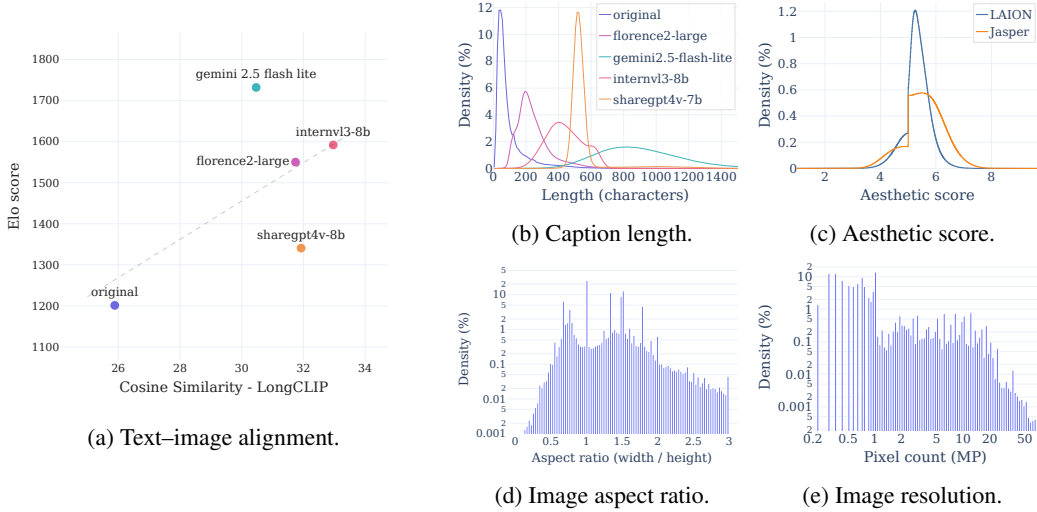


Figure 7: Captions and image statistics of MONET. Image resolution is in Megapixels (MP).

4 Dataset analysis

Caption & image statistics Fig. 7b shows the caption length distributions for the four retained captioners and the original captions. All generated captions are substantially longer than the originals, with Gemini-2.5-flash-lite producing the most verbose captions, followed by ShareGPT4V-7B and InternVL3-8B, while Florence2-Large produces compact captions (see Appendix A.3). Figs. 7c, 7d and 7e report the distributions of aesthetic score (LAION scores and scores from our internal classifier), aspect ratio and image resolution. Both aesthetic score distributions are centred in a similar interval, but our internal classifier exhibits greater spread, while LAION’s is more concentrated. Notably, both distributions show a sharp jump discontinuity at a score of 5, a result of the aesthetic pre-filtering of Sec. 3.2. Aspect ratios are mostly within $[0.5, 3.0]$, with clear peaks at common formats such as 1:1, 3:2, 2:1, and 3:4. Finally, most images are below 20 MP, although the distribution exhibits a long tail reaching up to 66 MP.

Content distribution To study the content distribution of MONET we explore two approaches: (i) top-5 YOLO object detections with COCO labels and (ii) CLIP-based zero-shot classification. Both YOLO outputs and CLIP embeddings are precomputed in Sec. 3 and stored in the dataset metadata. While YOLO provides structured detections, its expressiveness is limited by the COCO label space (80 object categories). For CLIP, we define $\sim 2.7k$ classes and encode them with the prompt “a photo of a {class}”, where {class} denotes the class name. Image-class similarities are computed via cosine similarity between image and text embeddings, and the top-5 classes are retained. Both YOLO and CLIP base classes are then grouped into two hierarchical meta-levels following Wu et al. [97] (see Appendix A.4.1). Fig. 8 (left) shows the dataset content distribution based on YOLO detections across the highest-level classes. The distribution is dominated by *objects* (41.3%) and *people* (35.3%), with smaller shares for *food and drink* (4.5%) and *design, art & graphics* (2.1%), reflecting the limited coverage of COCO labels (e.g. 10 food-related classes and a single relevant design class, “book”). Fig. 8 (middle) reports the CLIP-based distribution, which is more balanced: 25.3% *objects*, 22.5% *people*, 16.5% *nature*, 15.8% *urban*, 10.5% *food and drink* and 9.3% *design, art & graphics*. This improved coverage stems from the broader set of CLIP base classes, so we consider the CLIP-based estimates to be more representative of the dataset’s content. Overall, MONET’s distribution is consistent with comparable closed-source datasets: for example, Qwen-Image [97] reports 12.9% *people*, 21.7% *objects*, 27.4% *design*, 7.0% *food*, 13.6% *urban* and 12.5% *nature* (Animals, Landscapes and Plants). A detailed breakdown is provided in Appendix A.4.

Image style We use Qwen3-VL-8B-Instruct [105, 2] to classify a subset of the dataset, limited to 1.5M randomly sampled images for cost reasons, into 15 classes according to image style; the prompt and class definitions are provided in the Appendix A.4.2. Fig. 8 (right) shows the resulting

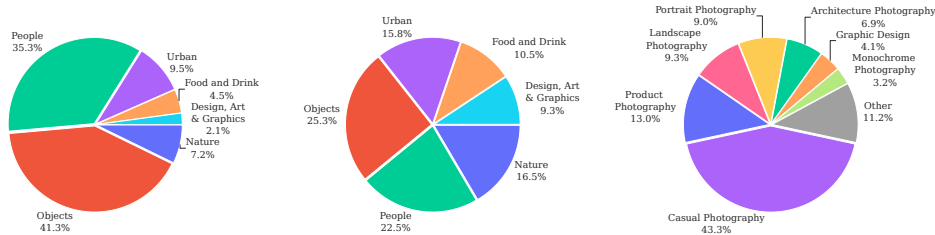


Figure 8: MONET dataset distribution: (left) YOLO-based content classification, (middle) CLIP-based content classification, (right) Qwen3-VL-8B-Instruct based image style.

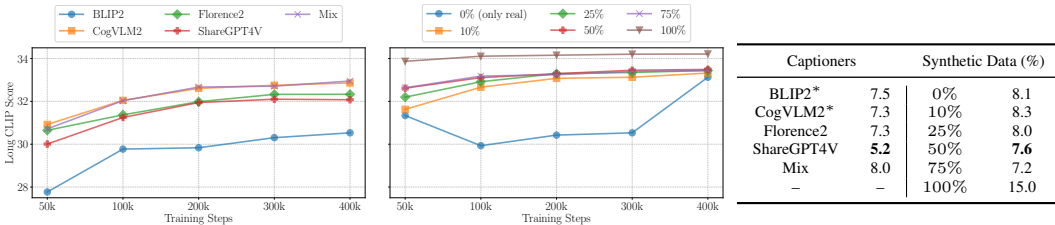


Figure 10: (Left) Long-CLIP score evolution throughout training with different captioning models and (middle) increasing amounts of synthetic data. (Right) FID scores computed after 400k training iterations on 50k samples from the ImageNet-512 validation set.

distribution. MONET spans a wide range of styles from graphic design and illustrations to portraits and product photography and is dominated by casual photography, a catch-all class for everyday photos. The full per-style distribution, including styles grouped under “Other”, is reported in Fig. 32.

5 Downstream validation

5.1 Impact of multi-captioning

To justify the decision to use multiple captioning models in MONET, we assess the impact of caption types on the performance of a T2I model. To do so we re-caption the ImageNet dataset [16] with four captioners of different complexity: BLIP2 [54], CogVLM2², Florence2 [100] and ShareGPT4V [13]. We then train five T2I diffusion models, one per captioner and one with captions uniformly sampled from all four (*Mix*); other training details are provided in Appendix A.5. We report in Fig. 10 (left) the Long-CLIP alignment score [107] and (right) the Fréchet Inception Distance (FID) [30] computed on 50k samples from the ImageNet-512 validation set, where evaluation captions are uniformly sampled from all four captioners. Our findings are in line with previous works [19, 97]: the use of multiple captioning models improves the robustness and generalization of the model. We additionally observe that a more verbose captioner, such as ShareGPT4V, accelerates convergence (lower FID), but that relying on a single captioner alone harms performance on out-of-distribution prompts motivating the multi-captioner mix used in MONET.

5.2 Impact of synthetic data

We conduct a similar experiment, varying the proportion of synthetic data added to the training set using the same diffusion-model architecture as in the previous experiment. We train six text-conditioned diffusion models on the original data set alone or the original data set augmented with synthetic samples generated by FLUX.2-klein-4B [49] in increasing proportions from 0 to 100% and evaluate them on the same validation set as in the previous section. As illustrated in Fig. 10 (middle), we observe that adding synthetic data improves text–image alignment, justifying the inclusion of

²We used BLIP2 and CogVLM2 captioners despite that they are not in the final MONET dataset since the benchmark of Sec. 3.6 was not performed at the time we launched this experiment.

Table 2: Results on the GenEval and DPG benchmarks. Our 4B model trained on the MONET dataset achieves competitive performance against models of similar size trained on closed-source data.

Model	Num. Params (B)	GenEval							DPG					
		Objects		Counting	Colors	Position	Color	Overall ↑	Global	Entity	Attribute	Relation	Other	Overall↑
Single	Two													
SD1.5 [76]	0.9	0.97	0.38	0.35	0.76	0.04	0.06	0.43	74.63	74.23	75.39	73.49	67.81	63.18
PixArt- α [10]	0.6	0.98	0.50	0.44	0.80	0.08	0.07	0.48	74.97	79.32	78.60	82.57	76.96	71.11
Emu3-Gen [96]	8.0	0.98	0.71	0.34	0.81	0.17	0.21	0.54	85.21	86.68	86.84	90.22	83.15	80.60
SDXL [68]	2.6	0.98	0.74	0.39	0.85	0.15	0.23	0.55	83.27	82.43	80.91	86.76	80.41	74.65
SD3 Medium [19]	2.0	0.98	0.74	0.63	0.67	0.34	0.36	0.62	87.90	91.01	88.83	80.70	88.68	84.08
FLUX.1 [Dev] [48]	12.0	0.98	0.81	0.74	0.79	0.22	0.45	0.66	74.35	90.00	88.96	90.87	88.33	83.84
DALL-E 3 [3]	–	0.96	0.87	0.47	0.83	0.43	0.45	0.67	90.97	89.61	88.39	90.58	89.83	83.50
SANA-1.5 [102]	4.8	0.99	0.85	0.77	0.87	0.34	0.54	0.72	–	–	–	–	–	85.00
Lumina-Image 2.0 [69]	2.6	–	0.87	0.67	–	–	0.62	0.73	–	91.97	90.20	94.85	–	87.20
Janus-Pro-7B [14]	7.0	0.99	0.89	0.59	0.90	0.79	0.66	0.80	86.90	88.90	89.40	89.32	89.48	84.19
HiDream-I1-Full [7]	17.0	1.00	0.98	0.79	0.91	0.60	0.72	0.83	76.44	90.22	89.48	93.74	91.83	85.89
Z-Image [106]	6.0	1.00	0.94	0.78	0.93	0.62	0.77	0.84	93.39	91.22	93.16	92.22	91.52	88.14
Qwen-Image [97]	20.0	0.99	0.92	0.89	0.88	0.76	0.77	0.87	91.32	91.56	92.02	94.31	92.73	88.32
Ours	4.1	1.00	0.90	0.73	0.88	0.35	0.62	0.74	84.80	91.76	89.70	94.16	79.60	85.56

such samples in MONET. However, as expected, an excessive synthetic ratio leads to overfitting or distribution shift, as evidenced by the markedly higher FID when training only on synthetic data.

5.3 Text-to-image model training

Finally, we train a 4B-parameter text-to-image model on MONET. We rely on the latent diffusion framework [76] with a denoiser inspired by MMDiT [19] and using a deep-compression VAE (DCVAE) [12]; text conditioning is injected using Qwen3-4B [105]. Table 2 reports the performance on the GenEval [25] and DPG [37] benchmarks of our model trained **exclusively** on MONET. As reported, the model is competitive with many existing models trained on closed-source data, underlining the quality of MONET. Qualitative samples generated at 1024×1024 resolution are shown in Fig. 11; additional 1024×1024 and 2048×2048 samples are provided in Appendix A.6.2. These samples illustrate the diversity and quality of MONET, supporting training even beyond the standard 1024^2 resolution. Full training details are provided in Appendix A.5.

6 Ethics & responsible use

Releasing a large-scale image–text dataset carries responsibilities regarding representation, safety and downstream impact. MONET aggregates web-sourced data we do not own; we therefore focus our ethical commitments on careful curation, transparent documentation, and the release of audit statistics to the community.

Representation audit. We audit a random sample of $\sim 5M$ images using Qwen3-VL-8B-Instruct with a structured prompt that elicits concrete visual evidence before committing to a categorical label, and defaults to *unknown* when evidence is insufficient (see full methodology, prompt and aggregate distributions in Appendix A.7). We focus on four demographic dimensions: *cultural origin*, *skin tone* (Fitzpatrick 1–6 [21]), *predominant gender* and *predominant age group*. Cultural origin is dominated by European and North American contexts, consistent with documented Western biases of web-scraped corpora [82]. Skin tones concentrate around categories 3–4, with lighter (1–2) and darker (5–6) tones under-represented; gender is roughly balanced, while age skews strongly toward adults, with children, teenagers and elderly subjects less frequent. These biases are largely inherited from the upstream sources, and the released annotations should help users re-weight the dataset toward a more balanced training distribution.

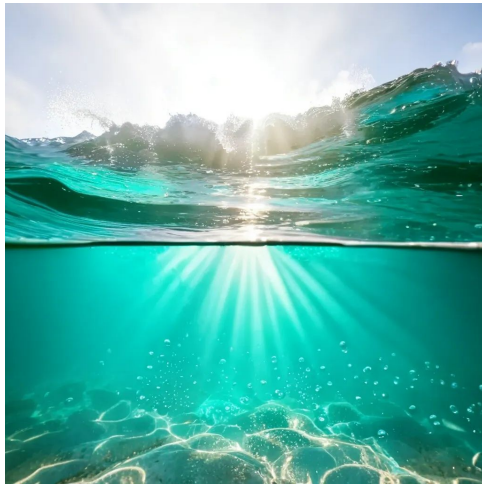
Responsible use. Despite our curation efforts, residual risks remain. The demographic biases above may propagate to models trained on MONET; practitioners should monitor outputs for fairness and apply mitigations such as balanced sampling. Safety filters do not achieve perfect recall, so downstream deployments should add output-level safety classifiers. We encourage users to follow ethical AI guidelines and consider the societal impact of derived models.



A transparent glass teapot filled with a miniature stormy ocean, tiny lightning bolts visible inside the glass.



A stunning landscape photograph captures the majestic Grand Canyon at sunrise or sunset, bathed in a warm, golden glow. The foreground is dominated by the rugged, layered cliffs of the canyon's edge, adorned with sparse but resilient trees and vegetation clinging to the rock faces.



A split-level shot (half underwater, half above) of a tropical turquoise wave breaking. Above water is misty spray; below water shows sunbeams (God rays) refracting through the moving surface, illuminating bubbles and sand.



A portrait of a samurai rendered in the style of a traditional 18th-century Japanese woodblock print, weathered paper texture.

Figure 11: Generation from our 4B model trained *exclusively* on MONET, showcasing its ability to learn complex concepts and a variety of styles at 1024×1024 and 2048×2048 resolutions.

7 Limitations and future work

MONET inherits biases from its Common-Crawl-based sources, over-representing European and North American contexts. Due to high compute requirements ($\sim 175\text{k}$ GPU-hours for the full pool), image-style and ethics-audit annotations are restricted to representative subsets and rely on a single VLM (Qwen3-VL-8B-Instruct). Extending the ethics annotations described in Sec. 6 to the full dataset would enable downstream re-weighting and the construction of a balanced dataset; scaling the process and cross-checking with other VLMs or human review are natural next steps for future work. MONET is English-only and re-captioning targets short, medium and long descriptions without structured attributes (counts, colours, spatial relations); multilingual captions and attribute-aware prompts are natural extensions. Synthetic content may also reflect hallucinations and stylistic biases of the underlying models, only partially mitigated by our multi-model mix. Moreover, our intentionally conservative *NSFW* and *watermark* filtering strategy could be at the expense of discarding *safe* and *compliant* images. Finally, our validation focuses on a 4B-parameter T2I model trained at up to 1024^2 resolution; scaling to larger models, higher resolutions and human preference studies is left to future work.

8 Conclusion

We introduced **MONET**, an open *Apache 2.0* dataset of **104.9M** curated image–text pairs built from heterogeneous open sources through successive stages of filtering, two-stage deduplication, multi-VLM re-captioning and synthetic-data augmentation, and shipped with pre-computed embeddings, annotations and latents to accelerate downstream use and deeper analysis. To the best of our knowledge, MONET is the first open, meticulously filtered, deduplicated and multi-captioned dataset for training T2I models at scale. We validated our design choices by training a 4B model that reaches competitive GenEval and DPG scores. MONET is also designed as a foundational *pre-training* dataset, intended to be paired with high-quality fine-tuning subsets for task-specific applications. By releasing MONET, we aim to lower the barrier to reproducible, large-scale text-to-image research.

References

- [1] Falcon AI. Fine-tuned vision transformer (vit) for nsfw image classification. https://huggingface.co/Falconsai/nsfw_image_detection, 2024. Accessed: 2026-04-16.
- [2] Jinze Bai, Shuai Bai, Shusheng Yang, Shijie Wang, Sinan Tan, Peng Wang, Junyang Lin, Chang Zhou, and Jingren Zhou. Qwen-vl: A versatile vision-language model for understanding, localization, text reading, and beyond. *arXiv preprint arXiv:2308.12966*, 2023.
- [3] James Betker, Gabriel Goh, Li Jing, Tim Brooks, Jianfeng Wang, Linjie Li, Long Ouyang, Juntang Zhuang, Joyce Lee, Yufei Guo, et al. Improving image generation with better captions. *Computer Science*. <https://cdn.openai.com/papers/dall-e-3.pdf>, 2(3):8, 2023.
- [4] Tom Brown, Benjamin Mann, Nick Ryder, Melanie Subbiah, Jared D Kaplan, Prafulla Dhariwal, Arvind Neelakantan, Pranav Shyam, Girish Sastry, Amanda Askell, et al. Language models are few-shot learners. *Advances in neural information processing systems*, 33:1877–1901, 2020.
- [5] Bumble-Tech. Bumble’s private detector model. <https://github.com/bumble-ai/nsfw-image-detection>, 2024. Accessed: 2026-04-16.
- [6] Minwoo Byeon, Beomhee Park, Haecheon Kim, Sungjun Lee, Woonhyuk Baek, and Saehoon Kim. Coyo-700m: Image-text pair dataset. <https://github.com/kakaobrain/coyo-dataset>, 2022.
- [7] Qi Cai, Jingwen Chen, Yang Chen, Yehao Li, Fuchen Long, Yingwei Pan, Zhaofan Qiu, Yiheng Zhang, Fengbin Gao, Peihan Xu, et al. Hidream-1l: A high-efficient image generative foundation model with sparse diffusion transformer. *arXiv preprint arXiv:2505.22705*, 2025.
- [8] Nicolas Carlini, Jamie Hayes, Milad Nasr, Matthew Jagielski, Vikash Sehwal, Florian Tramèr, Borja Balle, Daphne Ippolito, and Eric Wallace. Extracting training data from diffusion models. In *32nd USENIX security symposium (USENIX Security 23)*, pages 5253–5270, 2023.
- [9] Soravit Changpinyo, Piyush Sharma, Nan Ding, and Radu Soricut. Conceptual 12M: Pushing web-scale image-text pre-training to recognize long-tail visual concepts. In *CVPR*, 2021.
- [10] Junsong Chen, YU Jincheng, GE Chongjian, Lewei Yao, Enze Xie, Zhongdao Wang, James Kwok, Ping Luo, Huchuan Lu, and Zhenguo Li. Pixart- α : Fast training of diffusion transformer for photorealistic text-to-image synthesis. In *The Twelfth International Conference on Learning Representations*, 2023.
- [11] Junsong Chen, Chongjian Ge, Enze Xie, Yue Wu, Lewei Yao, Xiaozhe Ren, Zhongdao Wang, Ping Luo, Huchuan Lu, and Zhenguo Li. Pixart- σ : Weak-to-strong training of diffusion transformer for 4k text-to-image generation. *arXiv preprint arXiv:2403.04692*, 2024.
- [12] Junyu Chen, Han Cai, Junsong Chen, Enze Xie, Shang Yang, Haotian Tang, Muyang Li, and Song Han. Deep compression autoencoder for efficient high-resolution diffusion models. In *The Thirteenth International Conference on Learning Representations*, 2025.
- [13] Lin Chen, Jinsong Li, Xiaoyi Dong, Pan Zhang, Conghui He, Jiaqi Wang, Feng Zhao, and Dahua Lin. Sharegpt4v: Improving large multi-modal models with better captions. In *European Conference on Computer Vision*, pages 370–387. Springer, 2024.
- [14] Xiaokang Chen, Zhiyu Wu, Xingchao Liu, Zizheng Pan, Wen Liu, Zhenda Xie, Xingkai Yu, and Chong Ruan. Janus-pro: Unified multimodal understanding and generation with data and model scaling. *arXiv preprint arXiv:2501.17811*, 2025.
- [15] Gheorghe Comanici, Eric Bieber, Mike Schaekermann, Ice Pasupat, Noveen Sachdeva, Inderjit Dhillon, Marcel Blistein, Ori Ram, Dan Zhang, Evan Rosen, et al. Gemini 2.5: Pushing the frontier with advanced reasoning, multimodality, long context, and next generation agentic capabilities. *arXiv preprint arXiv:2507.06261*, 2025.
- [16] Jia Deng, Wei Dong, Richard Socher, Li-Jia Li, Kai Li, and Li Fei-Fei. Imagenet: A large-scale hierarchical image database. In *2009 IEEE conference on computer vision and pattern recognition*, pages 248–255. Ieee, 2009.
- [17] Karan Desai, Gaurav Kaul, Zubin Trivadi Aysola, and Justin Johnson. Redcaps: Web-curated image-text data created by the people, for the people. In *Thirty-fifth Conference on Neural Information Processing Systems Datasets and Benchmarks Track (Round 1)*, 2021. URL <https://openreview.net/forum?id=VjJxB1p9zh>.

- [18] Matthijs Douze, Alexandr Guzhva, Chengqi Deng, Jeff Johnson, Gergely Szilvasy, Pierre-Emmanuel Mazaré, Maria Lomeli, Lucas Hosseini, and Hervé Jegou. The faiss library. *arXiv preprint arXiv:2401.08281*, 2024.
- [19] Patrick Esser, Sumith Kulal, Andreas Blattmann, Rahim Entezari, Jonas Müller, Harry Saini, Yam Levi, Dominik Lorenz, Axel Sauer, Frederic Boesel, et al. Scaling rectified flow transformers for high-resolution image synthesis. *arXiv preprint arXiv:2403.03206*, 2024.
- [20] Alex Fang, Albin Madappally Jose, Amit Jain, Ludwig Schmidt, Alexander T Toshev, and Vaishaal Shankar. Data filtering networks. In *The Twelfth International Conference on Learning Representations*, 2024. URL <https://openreview.net/forum?id=KAk6ngZ09F>.
- [21] Thomas B Fitzpatrick. The validity and practicality of sun-reactive skin types I through VI. *Archives of Dermatology*, 124(6):869–871, 1988.
- [22] Samir Yitzhak Gadre, Gabriel Ilharco, Alex Fang, Jonathan Hayase, Georgios Smyrnis, Thao Nguyen, Ryan Marten, Mitchell Wortsman, Dhruva Ghosh, Jieyu Zhang, et al. Datacomp: In search of the next generation of multimodal datasets. *Advances in Neural Information Processing Systems*, 36:27092–27112, 2023.
- [23] Yu Gao, Lixue Gong, Qiushan Guo, Xiaoxia Hou, Zhichao Lai, Fanshi Li, Liang Li, Xiaochen Lian, Chao Liao, Liyang Liu, et al. Seedream 3.0 technical report. *arXiv preprint arXiv:2504.11346*, 2025.
- [24] Timnit Gebru, Jamie Morgenstern, Briana Vecchione, Jennifer Wortman Vaughan, Hanna Wallach, Hal Daumé III, and Kate Crawford. Datasheets for datasets. *Communications of the ACM*, 64(12):86–92, 2021.
- [25] Dhruva Ghosh, Hannaneh Hajishirzi, and Ludwig Schmidt. Geneval: An object-focused framework for evaluating text-to-image alignment. *Advances in Neural Information Processing Systems*, 36:52132–52152, 2023.
- [26] Aaron Gokaslan, A Feder Cooper, Jasmine Collins, Landan Seguin, Austin Jacobson, Mihir Patel, Jonathan Frankle, Cory Stephenson, and Volodymyr Kuleshov. Commoncanvas: An open diffusion model trained with creative-commons images. *arXiv preprint arXiv:2310.16825*, 2023.
- [27] Ian Goodfellow, Jean Pouget-Abadie, Mehdi Mirza, Bing Xu, David Warde-Farley, Sherjil Ozair, Aaron Courville, and Yoshua Bengio. Generative adversarial nets. In *Advances in Neural Information Processing Systems*, pages 2672–2680, 2014.
- [28] Aaron Grattafiori, Abhimanyu Dubey, Abhinav Jauhri, Abhinav Pandey, Abhishek Kadian, Ahmad Al-Dahle, Aiesha Letman, Akhil Mathur, Alan Schelten, Alex Vaughan, et al. The llama 3 herd of models. *arXiv preprint arXiv:2407.21783*, 2024.
- [29] Xiangming Gu, Chao Du, Tianyu Pang, Chongxuan Li, Min Lin, and Ye Wang. On memorization in diffusion models. *Transactions on Machine Learning Research*, 2025. ISSN 2835-8856. URL <https://openreview.net/forum?id=D3DBqvSDBj>.
- [30] Martin Heusel, Hubert Ramsauer, Thomas Unterthiner, Bernhard Nessler, and Sepp Hochreiter. Gans trained by a two time-scale update rule converge to a local nash equilibrium. *Advances in neural information processing systems*, 30, 2017.
- [31] Jonathan Ho and Tim Salimans. Classifier-free diffusion guidance. In *NeurIPS 2021 Workshop on Deep Generative Models and Downstream Applications*, 2021.
- [32] Jonathan Ho, Ajay Jain, and Pieter Abbeel. Denoising diffusion probabilistic models. *Advances in neural information processing systems*, 33:6840–6851, 2020.
- [33] Jonathan Ho, William Chan, Chitwan Saharia, Jay Whang, Ruiqi Gao, Alexey Gritsenko, Diederik P Kingma, Ben Poole, Mohammad Norouzi, David J Fleet, et al. Imagen video: High definition video generation with diffusion models. *arXiv preprint arXiv:2210.02303*, 2022.
- [34] Jordan Hoffmann, Sebastian Borgeaud, Arthur Mensch, Elena Buchatskaya, Trevor Cai, Eliza Rutherford, DDL Casas, Lisa Anne Hendricks, Johannes Welbl, Aidan Clark, et al. Training compute-optimal large language models. *arXiv preprint arXiv:2203.15556*, 10, 2022.
- [35] Wenyi Hong, Weihang Wang, Ming Ding, Wenmeng Yu, Qingsong Lv, Yan Wang, Yean Cheng, Shiyu Huang, Junhui Ji, Zhao Xue, et al. CogVLM2: Visual language models for image and video understanding. *arXiv preprint arXiv:2408.16500*, 2024.

- [36] Xiaowei Hu, Zhe Gan, Jianfeng Wang, Zhengyuan Yang, Zicheng Liu, Yumao Lu, and Lijuan Wang. Scaling up vision-language pre-training for image captioning. In *Proceedings of the IEEE/CVF conference on computer vision and pattern recognition*, pages 17980–17989, 2022.
- [37] Xiwei Hu, Rui Wang, Yixiao Fang, Bin Fu, Pei Cheng, and Gang Yu. Ella: Equip diffusion models with llm for enhanced semantic alignment. *arXiv preprint arXiv:2403.05135*, 2024.
- [38] Aaron Hurst, Adam Lerer, Adam P Goucher, Adam Perelman, Aditya Ramesh, Aidan Clark, AJ Ostrow, Akila Welihinda, Alan Hayes, Alec Radford, et al. Gpt-4o system card. *arXiv preprint arXiv:2410.21276*, 2024.
- [39] Chao Jia, Yinfei Yang, Ye Xia, Yi-Ting Chen, Zarana Parekh, Hieu Pham, Quoc Le, Yun-Hsuan Sung, Zhen Li, and Tom Duerig. Scaling up visual and vision-language representation learning with noisy text supervision. In *International conference on machine learning*, pages 4904–4916. PMLR, 2021.
- [40] Albert Q Jiang, Alexandre Sablayrolles, Antoine Roux, Arthur Mensch, Blanche Savary, Chris Bamford, Devendra Singh Chaplot, Diego de las Casas, Emma Bou Hanna, Florian Bressand, et al. Mixtral of experts. *arXiv preprint arXiv:2401.04088*, 2024.
- [41] Glenn Jocher, Ayush Chaurasia, and Jing Qiu. Ultralytics YOLOv8. <https://github.com/ultralytics/ultralytics>, 2023.
- [42] k-mktr. Improved FLUX prompts dataset. <https://huggingface.co/datasets/k-mktr/improved-flux-prompts>, 2024. Accessed: 2026-05-05.
- [43] Nikhil Kandpal, Eric Wallace, and Colin Raffel. Deduplicating training data mitigates privacy risks in language models. In *International Conference on Machine Learning*, pages 10697–10707. PMLR, 2022.
- [44] Minguk Kang, Jun-Yan Zhu, Richard Zhang, Jaesik Park, Eli Shechtman, Sylvain Paris, and Taesung Park. Scaling up gans for text-to-image synthesis. In *Proceedings of the IEEE/CVF Conference on Computer Vision and Pattern Recognition*, pages 10124–10134, 2023.
- [45] Diederik P Kingma and Jimmy Ba. Adam: A method for stochastic optimization. *arXiv preprint arXiv:1412.6980*, 2014.
- [46] Andreas Koukounas, Georgios Mastrapas, Michael Günther, Bo Wang, Scott Martens, Isabelle Mohr, Saba Sturua, Mohammad Kalim Akram, Joan Fontanals Martínez, Saahil Ognawala, et al. jina-clip-v2: Multilingual multimodal embeddings for text and images. *arXiv preprint arXiv:2412.08802*, 2024.
- [47] Ranjay Krishna, Yuke Zhu, Oliver Groth, Justin Johnson, Kenji Hata, Joshua Kravitz, Stephanie Chen, Yannis Kalantidis, Li-Jia Li, David A Shamma, et al. Visual genome: Connecting language and vision using crowdsourced dense image annotations. *International journal of computer vision*, 123(1):32–73, 2017.
- [48] Black Forest Labs. Flux. <https://github.com/black-forest-labs/flux>, 2024.
- [49] Black Forest Labs. FLUX.2: Frontier Visual Intelligence. <https://bfl.ai/blog/flux-2>, 2025.
- [50] LAION. Releasing re-laion-5b: transparent iteration on laion-5b with additional safety fixes. <https://laion.ai/blog/re-laion-5b/>, 2024. Accessed: 30 aug, 2024.
- [51] LAION-AI. Aesthetic predictor. <https://github.com/christophschuhmann/improved-aesthetic-predictor>, 2022. Accessed: 2026-04-03.
- [52] Katherine Lee, Daphne Ippolito, Andrew Nystrom, Chiyuan Zhang, Douglas Eck, Chris Callison-Burch, and Nicholas Carlini. Deduplicating training data makes language models better. In *Proceedings of the 60th Annual Meeting of the Association for Computational Linguistics (Volume 1: Long Papers)*, pages 8424–8445, 2022.
- [53] Daiqing Li, Aleks Kamko, Ehsan Akhgari, Ali Sabet, Linmiao Xu, and Suhail Doshi. Playground v2.5: Three insights towards enhancing aesthetic quality in text-to-image generation. *arXiv preprint arXiv:2402.17245*, 2024.
- [54] Junnan Li, Dongxu Li, Silvio Savarese, and Steven Hoi. Blip-2: Bootstrapping language-image pre-training with frozen image encoders and large language models. In *International conference on machine learning*, pages 19730–19742. PMLR, 2023.
- [55] Lijiang Li, Zuwei Long, Yunhang Shen, Heting Gao, Haoyu Cao, Xing Sun, Caifeng Shan, Ran He, and Chaoyou Fu. vunderstanding and generation with masked discrete diffusion. *arXiv preprint arXiv:2603.06577*, 2026.

- [56] Zhimin Li, Jianwei Zhang, Qin Lin, Jiangfeng Xiong, Yanxin Long, Xincheng Deng, Yingfang Zhang, Xingchao Liu, Minbin Huang, Zedong Xiao, et al. Hunyuan-dit: A powerful multi-resolution diffusion transformer with fine-grained chinese understanding. *arXiv preprint arXiv:2405.08748*, 2024.
- [57] Tsung-Yi Lin, Michael Maire, Serge Belongie, James Hays, Pietro Perona, Deva Ramanan, Piotr Dollár, and C Lawrence Zitnick. Microsoft coco: Common objects in context. In *Computer Vision—ECCV 2014: 13th European Conference, Zurich, Switzerland, September 6-12, 2014, Proceedings, Part V 13*, pages 740–755. Springer, 2014.
- [58] Yaron Lipman, Ricky TQ Chen, Heli Ben-Hamu, Maximilian Nickel, and Matthew Le. Flow matching for generative modeling. In *The Eleventh International Conference on Learning Representations*, 2023.
- [59] Aixin Liu, Bei Feng, Bing Xue, Bingxuan Wang, Bochao Wu, Chengda Lu, Chenggang Zhao, Chengqi Deng, Chenyu Zhang, Chong Ruan, et al. Deepseek-v3 technical report. *arXiv preprint arXiv:2412.19437*, 2024.
- [60] Xingchao Liu, Chengyue Gong, et al. Flow straight and fast: Learning to generate and transfer data with rectified flow. In *The Eleventh International Conference on Learning Representations*, 2022.
- [61] Camillo Lugaresi, Jiuqiang Tang, Hadon Nash, Chris McClanahan, Esha Uboweja, Michael Hays, Fan Zhang, Chuo-Ling Chang, Ming Guang Yong, Juhyun Lee, et al. MediaPipe: A framework for building perception pipelines. *arXiv preprint arXiv:1906.08172*, 2019.
- [62] Yiyang Ma, Xingchao Liu, Xiaokang Chen, Wen Liu, Chengyue Wu, Zhiyu Wu, Zizheng Pan, Zhenda Xie, Haowei Zhang, Xingkai Yu, et al. v: Harmonizing autoregression and rectified flow for unified multimodal understanding and generation. In *Proceedings of the IEEE/CVF Conference on Computer Vision and Pattern Recognition*, pages 7739–7751, 2025.
- [63] OpenAI. Gpt-image-1, 2025. URL <https://openai.com/zh-Hans-CN/index/introducing-gpt-4o-image-generation/>.
- [64] Maxime Oquab, Timothée Darcet, Théo Moutakanni, Huy Vo, Marc Szafraniec, Vasil Khalidov, Pierre Fernandez, Daniel Haziza, Francisco Massa, Alaaeldin El-Nouby, et al. Dinov2: Learning robust visual features without supervision. *Transactions on Machine Learning Research*, 2024.
- [65] William Peebles and Saining Xie. Scalable diffusion models with transformers. In *Proceedings of the IEEE/CVF International Conference on Computer Vision*, pages 4195–4205, 2023.
- [66] Ed Pizzi, Sreya Dutta Roy, Sugosh Nagavara Ravindra, Priya Goyal, and Matthijs Douze. A self-supervised descriptor for image copy detection. *Proc. CVPR*, 2022.
- [67] Ed Pizzi, Sreya Dutta Roy, Sugosh Nagavara Ravindra, Priya Goyal, and Matthijs Douze. SSCD: A self-supervised descriptor for image copy detection – code and pretrained models. <https://github.com/facebookresearch/sscd-copy-detection>, 2022. Accessed: 2026-04-23.
- [68] Dustin Podell, Zion English, Kyle Lacey, Andreas Blattmann, Tim Dockhorn, Jonas Müller, Joe Penna, and Robin Rombach. Sdxl: Improving latent diffusion models for high-resolution image synthesis. In *The Twelfth International Conference on Learning Representations*, 2023.
- [69] Qi Qin, Le Zhuo, Yi Xin, Ruoyi Du, Zhen Li, Bin Fu, Yiting Lu, Xinyue Li, Dongyang Liu, Xiangyang Zhu, et al. Lumina-image 2.0: A unified and efficient image generative framework. In *Proceedings of the IEEE/CVF International Conference on Computer Vision*, pages 20031–20042, 2025.
- [70] Alec Radford, Jong Wook Kim, Chris Hallacy, Aditya Ramesh, Gabriel Goh, Sandhini Agarwal, Girish Sastry, Amanda Askell, Pamela Mishkin, Jack Clark, et al. Learning transferable visual models from natural language supervision. In *International conference on machine learning*, pages 8748–8763. PMLR, 2021.
- [71] Colin Raffel, Noam Shazeer, Adam Roberts, Katherine Lee, Sharan Narang, Michael Matena, Yanqi Zhou, Wei Li, and Peter J Liu. Exploring the limits of transfer learning with a unified text-to-text transformer. *Journal of machine learning research*, 21(140):1–67, 2020.
- [72] Aditya Ramesh, Mikhail Pavlov, Gabriel Goh, Scott Gray, Chelsea Voss, Alec Radford, Mark Chen, and Ilya Sutskever. Zero-shot text-to-image generation. In *International conference on machine learning*, pages 8821–8831. Pmlr, 2021.
- [73] Aditya Ramesh, Prafulla Dhariwal, Alex Nichol, Casey Chu, and Mark Chen. Hierarchical text-conditional image generation with clip latents. *arXiv preprint arXiv:2204.06125*, 2022.

- [74] Anton Razhigaev, Arseniy Shakhmatov, Anastasia Maltseva, Vladimir Arkhipkin, Igor Pavlov, Ilya Ryabov, Angelina Kuts, Alexander Panchenko, Andrey Kuznetsov, and Denis Dimitrov. Kandinsky: an improved text-to-image synthesis with image prior and latent diffusion. In *Proceedings of the 2023 Conference on Empirical Methods in Natural Language Processing: System Demonstrations*, pages 286–295, 2023.
- [75] Joseph Redmon, Santosh Divvala, Ross Girshick, and Ali Farhadi. You only look once: Unified, real-time object detection. In *CVPR*, pages 779–788, 2016.
- [76] Robin Rombach, Andreas Blattmann, Dominik Lorenz, Patrick Esser, and Björn Ommer. High-resolution image synthesis with latent diffusion models. In *Proceedings of the IEEE/CVF conference on computer vision and pattern recognition*, pages 10684–10695, 2022.
- [77] Olaf Ronneberger, Philipp Fischer, and Thomas Brox. U-net: Convolutional networks for biomedical image segmentation. In *Medical image computing and computer-assisted intervention—MICCAI 2015: 18th international conference, Munich, Germany, October 5-9, 2015, proceedings, part III 18*, pages 234–241. Springer, 2015.
- [78] Chitwan Saharia, William Chan, Saurabh Saxena, Lala Li, Jay Whang, Emily L Denton, Kamyar Ghasemipour, Raphael Gontijo Lopes, Burcu Karagol Ayan, Tim Salimans, et al. Photorealistic text-to-image diffusion models with deep language understanding. *Advances in neural information processing systems*, 35:36479–36494, 2022.
- [79] Axel Sauer, Tero Karras, Samuli Laine, Andreas Geiger, and Timo Aila. Stylegan-t: Unlocking the power of gans for fast large-scale text-to-image synthesis. In *International conference on machine learning*, pages 30105–30118. PMLR, 2023.
- [80] Axel Sauer, Dominik Lorenz, Andreas Blattmann, and Robin Rombach. Adversarial diffusion distillation. *arXiv preprint arXiv:2311.17042*, 2023.
- [81] Christoph Schuhmann, Richard Vencu, Romain Beaumont, Robert Kaczmarczyk, Clayton Mullis, Aarush Katta, Theo Coombes, Jenia Jitsev, and Aran Komatsuzaki. Laion-400m: Open dataset of clip-filtered 400 million image-text pairs. *arXiv preprint arXiv:2111.02114*, 2021.
- [82] Christoph Schuhmann, Romain Beaumont, Richard Vencu, Cade Gordon, Ross Wightman, Mehdi Cherti, Theo Coombes, Aarush Katta, Clayton Mullis, Mitchell Wortsman, et al. Laion-5b: An open large-scale dataset for training next generation image-text models. *Advances in Neural Information Processing Systems*, 35:25278–25294, 2022.
- [83] Piyush Sharma, Nan Ding, Sebastian Goodman, and Radu Soricut. Conceptual captions: A cleaned, hypernymed, image alt-text dataset for automatic image captioning. In *Proceedings of the 56th Annual Meeting of the Association for Computational Linguistics (Volume 1: Long Papers)*, pages 2556–2565, 2018.
- [84] Jascha Sohl-Dickstein, Eric Weiss, Niru Maheswaranathan, and Surya Ganguli. Deep unsupervised learning using nonequilibrium thermodynamics. In *International conference on machine learning*, pages 2256–2265. PMLR, 2015.
- [85] Gowthami Somepalli, Vasu Singla, Micah Goldblum, Jonas Geiping, and Tom Goldstein. Diffusion art or digital forgery? investigating data replication in diffusion models. In *Proceedings of the IEEE/CVF conference on computer vision and pattern recognition*, pages 6048–6058, 2023.
- [86] Yang Song, Jascha Sohl-Dickstein, Diederik P Kingma, Abhishek Kumar, Stefano Ermon, and Ben Poole. Score-based generative modeling through stochastic differential equations. In *International Conference on Learning Representations*, 2020.
- [87] Alexander Swerdlow, Mihir Prabhudesai, Siddharth Gandhi, Deepak Pathak, and Katerina Fragkiadaki. Unified multimodal discrete diffusion. *arXiv preprint arXiv:2503.20853*, 2025.
- [88] Chameleon Team. Chameleon: Mixed-modal early-fusion foundation models. *arXiv preprint arXiv:2405.09818*, 2024.
- [89] Gemini Team, Petko Georgiev, Ving Ian Lei, Ryan Burnell, Libin Bai, Anmol Gulati, Garrett Tanzer, Damien Vincent, Zhufeng Pan, Shibo Wang, et al. Gemini 1.5: Unlocking multimodal understanding across millions of tokens of context. *arXiv preprint arXiv:2403.05530*, 2024.
- [90] Bart Thomee, David A Shamma, Gerald Friedland, Benjamin Elizalde, Karl Ni, Douglas Poland, Damian Borth, and Li-Jia Li. Yfcc100m: The new data in multimedia research. *Communications of the ACM*, 59(2):64–73, 2016.

- [91] Michael Tschanen, Alexey Gritsenko, Xiao Wang, Muhammad Ferjad Naeem, Ibrahim Alabdulmohsin, Nikhil Parthasarathy, Talfan Evans, Lucas Beyer, Ye Xia, Basil Mustafa, Olivier Hénaff, Jeremiah Harmsen, Andreas Steiner, and Xiaohua Zhai. SigLIP 2: Multilingual vision-language encoders with improved semantic understanding, localization, and dense features. *arXiv preprint arXiv:2502.14786*, 2025.
- [92] Pavan Kumar Anasosalu Vasu, Fartash Faghri, Chun-Liang Li, Cem Koc, Nate True, Albert Antony, Gokula Santhanam, James Gabriel, Peter Grasch, Oncel Tuzel, et al. Fastvlm: Efficient vision encoding for vision language models. In *Proceedings of the Computer Vision and Pattern Recognition Conference*, pages 19769–19780, 2025.
- [93] Ashish Vaswani, Noam Shazeer, Niki Parmar, Jakob Uszkoreit, Llion Jones, Aidan N Gomez, Łukasz Kaiser, and Illia Polosukhin. Attention is all you need. *Advances in neural information processing systems*, 30, 2017.
- [94] Ramarathnam Venkatesan, S-M Koon, Mariusz H Jakubowski, and Pierre Moulin. Robust image hashing. In *Proceedings 2000 International Conference on Image Processing (Cat. No. 00CH37101)*, volume 3, pages 664–666. IEEE, 2000.
- [95] Weihang Wang, Qingsong Lv, Wenmeng Yu, Wenyi Hong, Ji Qi, Yan Wang, Junhui Ji, Zhuoyi Yang, Lei Zhao, Xixuan Song, et al. Cogvlm: Visual expert for pretrained language models. *Advances in Neural Information Processing Systems*, 37:121475–121499, 2024.
- [96] Xinlong Wang, Xiaosong Zhang, Zhengxiong Luo, Quan Sun, Yufeng Cui, Jinsheng Wang, Fan Zhang, Yueze Wang, Zhen Li, Qiyang Yu, et al. Emu3: Next-token prediction is all you need. *arXiv preprint arXiv:2409.18869*, 2024.
- [97] Chenfei Wu, Jiahao Li, Jingren Zhou, Junyang Lin, Kaiyuan Gao, Kun Yan, Sheng-ming Yin, Shuai Bai, Xiao Xu, Yilei Chen, et al. Qwen-image technical report. *arXiv preprint arXiv:2508.02324*, 2025.
- [98] Chengyue Wu, Xiaokang Chen, Zhiyu Wu, Yiyang Ma, Xingchao Liu, Zizheng Pan, Wen Liu, Zhenda Xie, Xingkai Yu, Chong Ruan, et al. Janus: Decoupling visual encoding for unified multimodal understanding and generation. In *Proceedings of the Computer Vision and Pattern Recognition Conference*, pages 12966–12977, 2025.
- [99] Yecheng Wu, Zhuoyang Zhang, Junyu Chen, Haotian Tang, Dacheng Li, Yunhao Fang, Ligeng Zhu, Enze Xie, Hongxu Yin, Li Yi, et al. Vila-u: a unified foundation model integrating visual understanding and generation. In *The Thirteenth International Conference on Learning Representations*, 2025.
- [100] Bin Xiao, Haiping Wu, Weijian Xu, Xiyang Dai, Houdong Hu, Yumao Lu, Michael Zeng, Ce Liu, and Lu Yuan. Florence-2: Advancing a unified representation for a variety of vision tasks. In *2024 IEEE/CVF Conference on Computer Vision and Pattern Recognition (CVPR)*, pages 4818–4829. IEEE Computer Society, 2024.
- [101] Enze Xie, Junsong Chen, Junyu Chen, Han Cai, Haotian Tang, Yujun Lin, Zhekai Zhang, Muyang Li, Ligeng Zhu, Yao Lu, et al. Sana: Efficient high-resolution image synthesis with linear diffusion transformers. *arXiv preprint arXiv:2410.10629*, 2024.
- [102] Enze Xie, Junsong Chen, Yuyang Zhao, Jincheng Yu, Ligeng Zhu, Yujun Lin, Zhekai Zhang, Muyang Li, Junyu Chen, Han Cai, et al. Sana 1.5: Efficient scaling of training-time and inference-time compute in linear diffusion transformer. In *International Conference on Machine Learning*, pages 68578–68598. PMLR, 2025.
- [103] Jinheng Xie, Weijia Mao, Zechen Bai, David Junhao Zhang, Weihao Wang, Kevin Qinghong Lin, Yuchao Gu, Zhijie Chen, Zhenheng Yang, and Mike Zheng Shou. Show-o: One single transformer to unify multimodal understanding and generation. In *The Thirteenth International Conference on Learning Representations*, 2025.
- [104] Tao Xu, Pengchuan Zhang, Qiuyuan Huang, Han Zhang, Zhe Gan, Xiaolei Huang, and Xiaodong He. Attngan: Fine-grained text to image generation with attentional generative adversarial networks. In *Proceedings of the IEEE conference on computer vision and pattern recognition*, pages 1316–1324, 2018.
- [105] An Yang, Anfeng Li, Baosong Yang, Beichen Zhang, Binyuan Hui, Bo Zheng, Bowen Yu, Chang Gao, Chengen Huang, Chenxu Lv, et al. Qwen3 technical report. *arXiv preprint arXiv:2505.09388*, 2025.
- [106] Z-Image Team. Z-image: An efficient image generation foundation model with single-stream diffusion transformer. *arXiv preprint arXiv:2511.22699*, 2025.

- [107] Beichen Zhang, Pan Zhang, Xiaoyi Dong, Yuhang Zang, and Jiaqi Wang. Long-clip: Unlocking the long-text capability of clip. In *European conference on computer vision*, pages 310–325. Springer, 2024.
- [108] Jinjin Zhang, Qiuyu Huang, Junjie Liu, Xiefan Guo, and Di Huang. Diffusion-4k: Ultra-high-resolution image synthesis with latent diffusion models. In *IEEE/CVF Conference on Computer Vision and Pattern Recognition (CVPR)*, 2025.
- [109] Chuyang Zhao, Yuxing Song, Wenhao Wang, Haocheng Feng, Errui Ding, Yifan Sun, Xinyan Xiao, and Jingdong Wang. Monoformer: One transformer for both diffusion and autoregression. *arXiv preprint arXiv:2409.16280*, 2024.
- [110] Chunting Zhou, Pengfei Liu, Puxin Xu, Srinivasan Iyer, Jiao Sun, Yuning Mao, Xuezhe Ma, Avia Efrat, Ping Yu, Lili Yu, et al. Lima: Less is more for alignment. *Advances in Neural Information Processing Systems*, 36:55006–55021, 2023.
- [111] Chunting Zhou, LILI YU, Arun Babu, Kushal Tirumala, Michihiro Yasunaga, Leonid Shamis, Jacob Kahn, Xuezhe Ma, Luke Zettlemoyer, and Omer Levy. Transfusion: Predict the next token and diffuse images with one multi-modal model. In *The Thirteenth International Conference on Learning Representations*, 2025.
- [112] Jinguo Zhu, Weiyun Wang, Zhe Chen, Zhaoyang Liu, Shenglong Ye, Lixin Gu, Hao Tian, Yuchen Duan, Weijie Su, Jie Shao, et al. Internvl3: Exploring advanced training and test-time recipes for open-source multimodal models. *arXiv preprint arXiv:2504.10479*, 2025.
- [113] Le Zhuo, Ruoyi Du, Han Xiao, Yangguang Li, Dongyang Liu, Rongjie Huang, Wenze Liu, Lirui Zhao, Fu-Yun Wang, Zhanyu Ma, et al. Lumina-next: Making lumina-t2x stronger and faster with next-dit. *arXiv preprint arXiv:2406.18583*, 2024.

A Technical appendices and supplementary material

Contents

A.1	Filtering details	21
A.2	Deduplication details	25
A.3	Re-captioning with VLMs	31
A.4	Details on image content and style classifications	38
A.5	Training details	44
A.6	Additional results	45
A.7	Ethics audit	51
A.8	Datasheet	53

A.1 Filtering details

In this section, we detail the domain-based (URL and watermark) and NSFW filters used. These act as exclusion controls and source-governance signals, not as a representation of legal clearance.

A.1.1 URL filtering

URL filtering removes any image whose URL contains the name of a known stock photo provider (Dreamstime, Shutterstock, Freepik, Getty, Unsplash, Pexels, etc). Table 3 reports the number of removed images and their proportion of the overall dataset, broken down by source and domain. We observed that some filtered images clearly display watermarks (such as those from Dreamstime, Shutterstock, and Getty) which validate the filtering approach. However, most images from Unsplash and Pexels, as well as some from Getty, do not include watermarks, which would make filtering at a later stage more difficult.

Table 3: Number and proportion of removed images by URL-based filtering across stock image domains.

Source	Domain	Removed images	Percentage
Dreamstime	dreamstime.com	1,387,253	1.16%
Shutterstock	image.shutterstock.com	215,833	0.18%
Freepik	freepik.com	168,665	0.16%
Getty	media.gettyimages.com	167,141	0.14%
Unsplash	unsplash.com	162,429	0.14%
Pexels	pexels.com	96,361	0.08%
Envato	envato.com	33,150	0.03%
Adobe Stock / Fotolia	stock.adobe.com	25,970	0.02%
Vecteezy	vecteezy.com	15,410	0.01%
123RF	123rf.com	13,536	0.01%
Depositphotos	depositphotos.com	8,609	0.01%
Pixabay	pixabay.com	8,191	0.01%
Reuters Pictures	reuters.com	6,155	0.01%
AFP	afp.com	4,746	0.00%
Creative Market	creativemarket.com	1,654	0.00%
iStock	istockphoto.com	887	0.00%
Alamy	alamy.com	854	0.00%
Pond5	pond5.com	340	0.00%
Bigstock	bigstockphoto.com	108	0.00%
Storyblocks	storyblocks.com	74	0.00%
AP Images	apimages.com	27	0.00%
Zuma / Newscom / Rex	zumapress.com	1	0.00%

A.1.2 Watermark filtering

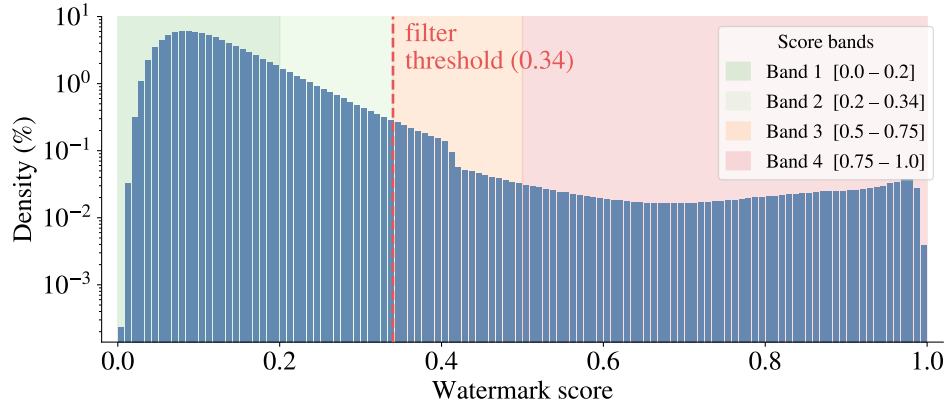
Watermark filtering is achieved by running an internal watermark detector through the entire dataset, which produces a continuous score ranging from 0 to 1, where 1 indicates the highest likelihood of a watermark. Images are then filtered based on a manually tuned threshold; in this case, the cut-off is set to 0.34.

Fig. 12a shows the histogram of the watermark filter scores in logarithmic scale, together with the filter threshold. The scores were divided into four score bands or intervals, two of which consist of retained images and two of filtered images, and one example per score brand is showcased (Figs. 12b, 12c, 12d, 12e). Images in the two retained bands show no visible watermarks. We observe that band 3 typically contains more subtle watermarks, such as a single watermark in the bottom-right corner (Fig. 12e), while band 4 includes images with multiple watermarks (see Fig. 12d).

A.1.3 NSFW filtering

Three distinct methods are used to filter NSFW content: an internal (Jasper) NSFW detector and two publicly available detectors, Bumble and Falcon. Both Jasper and Bumble produce a continuous NSFW score for each image, and images with scores exceeding a specified threshold are discarded. The threshold for Jasper is manually tuned, whereas for Bumble the threshold recommended by the authors is adopted [5]. Falcon, in contrast, outputs a binary NSFW label, where 0 denotes safe content and 1 denotes NSFW content.

Fig. 13 shows the histogram of the Jasper NSFW scores with some examples. The histogram is divided into 5 score bands, the first consisting of retained images, while the latter three consist of rejected images. Examples of the first four bands are shown in Figs. 13b–13e, while no example from the fifth band is included due to its highly explicit NSFW content. As illustrated, the content transitions smoothly from clearly safe material to progressively more NSFW content. We note that the cut-off threshold is intentionally conservative, and that images filtered near this boundary, i.e., band 3 images, are only mildly unsafe.



(a) Histogram in logarithmic scale, with filtering threshold.



(b) Band 1 (retained)



(c) Band 2 (retained)



(d) Band 3 (filtered)

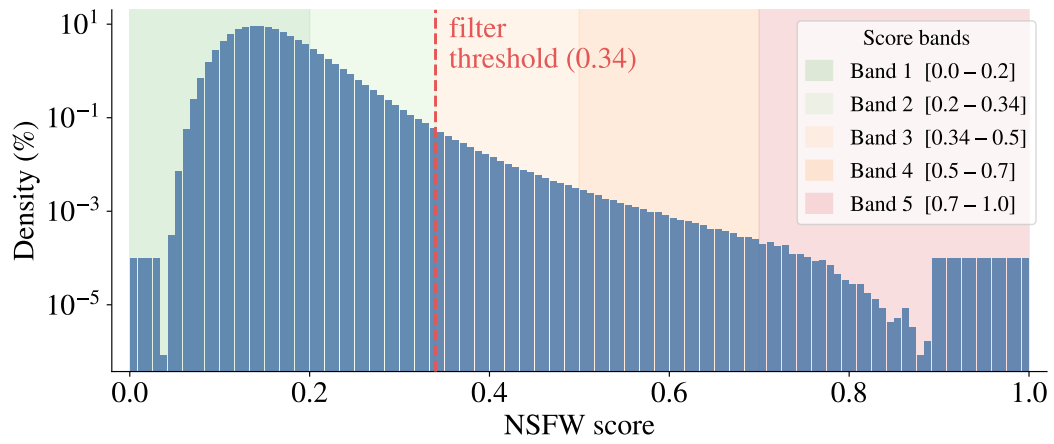


(e) Band 4 (filtered)

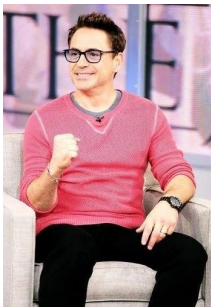
Figure 12: Distribution and examples of watermark scores.

Fig. 14 presents the score distribution for Bumble, divided into five score bands, along with representative examples for the first four bands. Again, no example from the last band is showed due to its explicit NSFW content. As before, the progression from safe images to NSFW content appears gradual. Band 3, illustrated in Fig. 14d, consists mainly of mildly unsafe or even safe images, where nudity is typically associated with sculptures and paintings.

Finally, Fig. 15 shows the distribution of Falcon predictions. Since this detector is binary, we do not include any example due to some highly explicit NSFW content being detected. Nonetheless, this detector appears highly conservative, as many of the rejected images are only mildly unsafe or not clearly unsafe at all.



(a) Histogram in logarithmic scale, with filtering threshold.



(b) Band 1 (retained)



(c) Band 2 (retained)

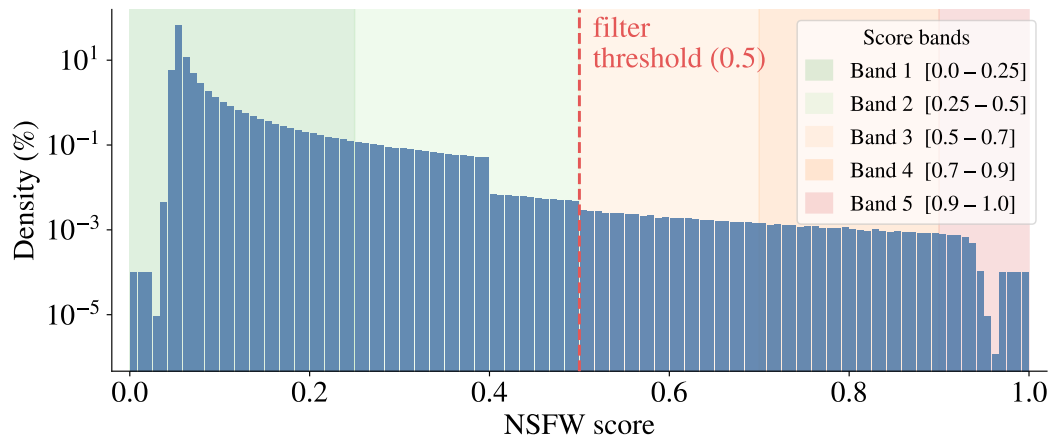


(d) Band 3 (filtered)



(e) Band 4 (filtered)

Figure 13: Distribution and examples of Jasper NSFW score. No band 5 examples are included.



(a) Histogram in logarithmic scale, with filtering threshold.



Figure 14: Distribution and examples of Bumble NSFW score.

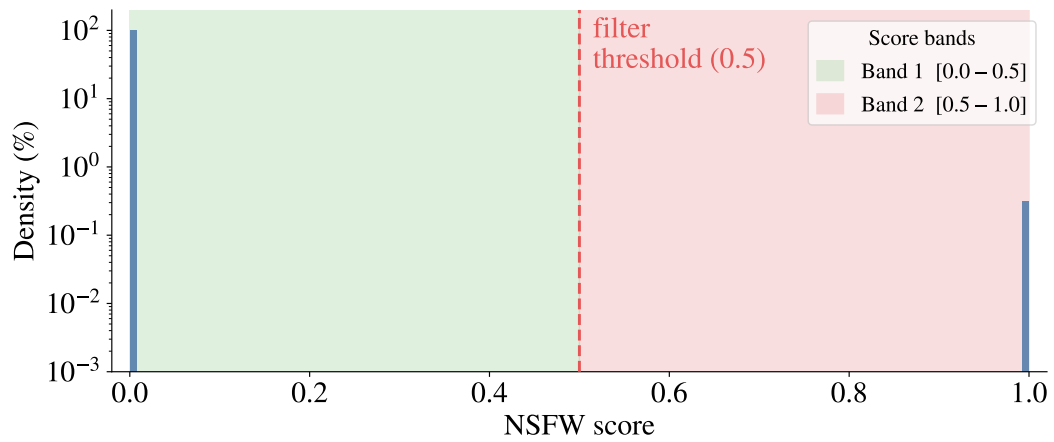


Figure 15: Histogram in logarithmic scale, with filtering threshold.

A.2 Deduplication details

A.2.1 Perceptual hashing

We use the DCT-based perceptual hash (pHash) of Venkatesan et al. [94] as our first-pass duplicate detector. Each image is converted to grayscale, resized to 32×32 , and transformed by a 2D DCT; the top-left 8×8 block of low-frequency coefficients is binarized against the median, yielding a 64-bit fingerprint. Pairs are compared by the Hamming distance d between their hashes.

In our pipeline, pHash is applied both *intra-source* during merging and *inter-source* after consolidation, removing approximately 19.7M and 1.9M images respectively. Because the hash discards high-frequency content, it is robust to mild JPEG re-compression, resizing, and small overlays, but sensitive to flips, crops, and color shifts. Fig. 16 shows representative clusters at three operating points: *i.e.* $d = 0$ pairs are exact-hash matches, at $d = 2$ they are visually indistinguishable copies that differ only in compression or minor pixel-level edits, and at $d = 4$ the clusters still capture re-encodings of the same image with slight variations in resolution or color grading.

However, when d increases, pHash starts to mix genuine duplicates with semantically unrelated images that share a similar global layout, since the 64-bit fingerprint only encodes a coarse spatial frequency representation of the image. Fig. 17 illustrates such false-positive clusters: horizontal stripe patterns, small objects on a uniform background (a bee, a bird, a motocross rider, a coffee mug), and centered products on a white background (a pill icon, a shoe, an SD card). To recover from these failure modes while still catching transformations that defeat low-frequency hashing (flips, large crops, color shifts, watermark insertion), we use a learned embedding (SSCD) for the second pass.

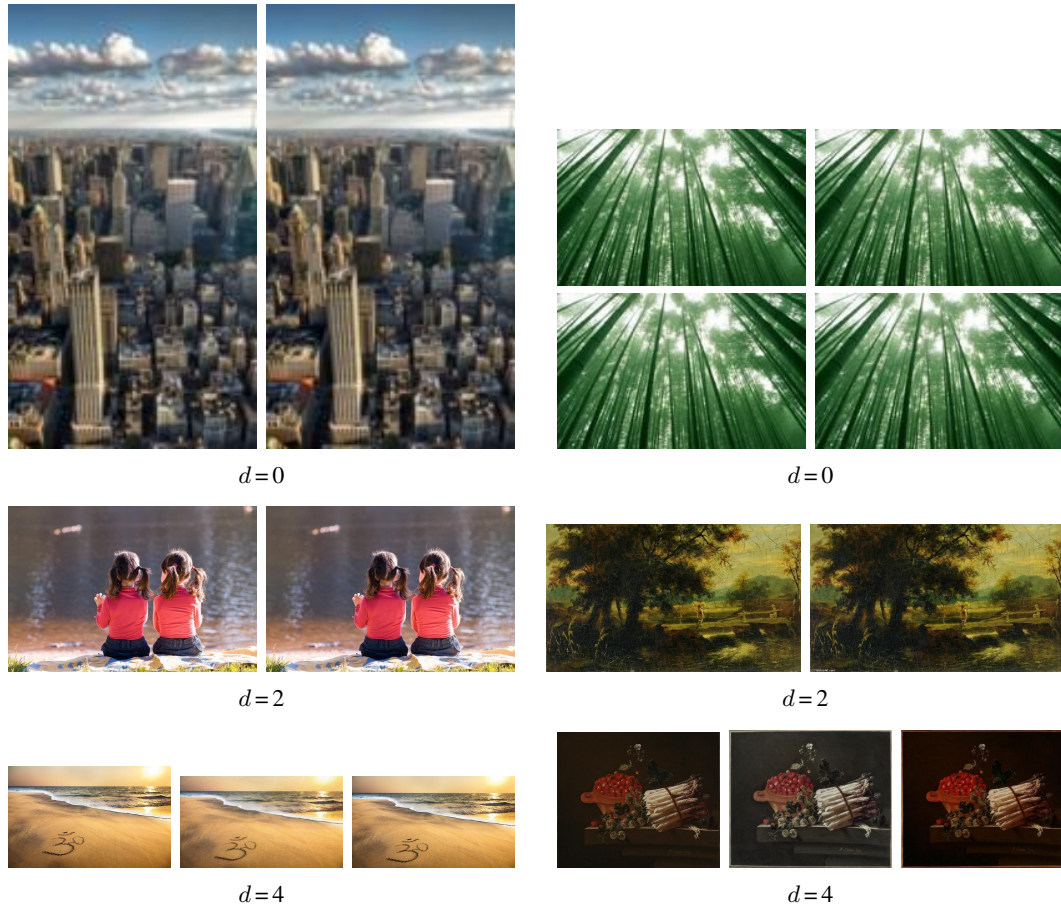
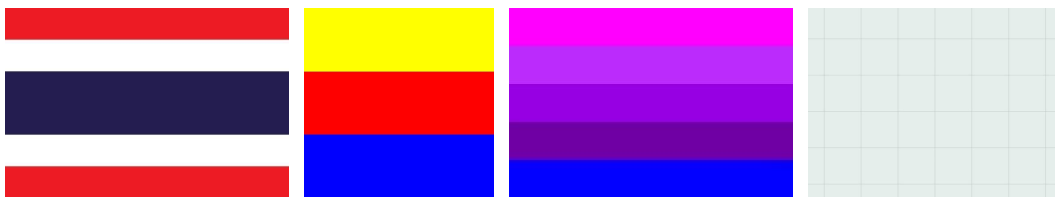
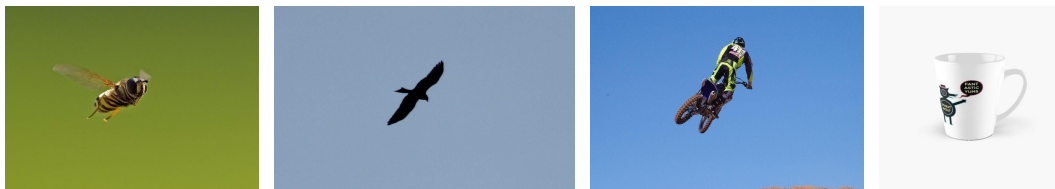


Figure 16: Duplicate clusters detected by perceptual hashing at increasing Hamming distance d . Best viewed zoomed in.



Cluster A: horizontal stripe patterns



Cluster B: small object on uniform background



Cluster C: centered object on white background

Figure 17: pHash false positive clusters: each row shows images that pHash assigns a low Hamming distance $d = 1$, yet the images are semantically unrelated. pHash conflates global color distributions and coarse spatial layout with perceptual identity.

A.2.2 SSCD

To complement pHash and capture transformations that defeat low-frequency hashing such as horizontal flips, large crops, color and tone shifts, watermark insertion, or background substitution, we use Self-Supervised Copy Detection (SSCD) embeddings [66]. We use the public `sscd_disc_mixup` checkpoint [67], which produces a 512-dimensional descriptor explicitly trained for copy detection. Embeddings are L2-normalized, indexed with FAISS [18], and for every image we retrieve its $k = 64$ nearest neighbors. Pairs with cosine similarity ≥ 0.75 are merged into clusters via union-find, and within each cluster we keep a single representative chosen by the highest combined resolution and aesthetic score for possible ties; the remaining members are discarded. This stage removes an additional 5.22M images.

Fig. 18 reports the distribution of nearest-neighbor cosine similarities over the deduplicated pool. The distribution is bimodal: a heavy mass below ~ 0.5 corresponding to genuinely distinct images, and a long tail towards 1.0 populated by near-duplicates. The 0.75 operating point recommended by the SSCD authors [67] (90% precision on DISC), which we further validate by manually inspecting random pair slices in 0.05-wide bins (cf. Fig. 4 of the main paper and Fig. 19): above 0.75 neighbors are consistently near-duplicates, whereas below 0.75 they are merely semantically related.

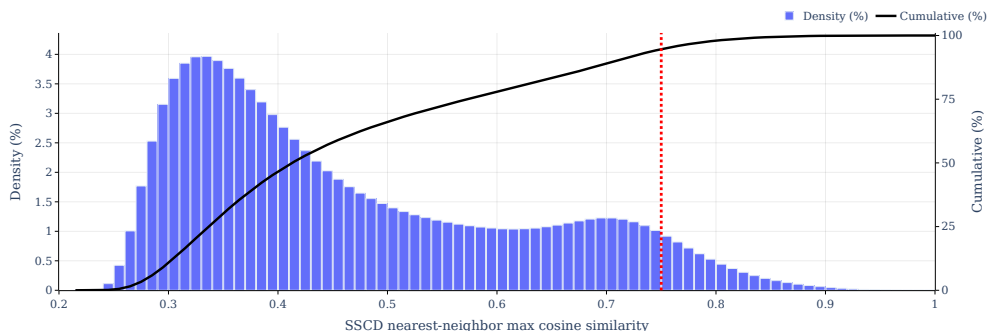


Figure 18: Distribution of SSCD nearest-neighbor maximum cosine similarities.



Figure 19: SSCD threshold sweep. Nearest-neighbor pairs sampled at increasing cosine similarity. For low SSCD, pairs are merely semantically related (different photos from the same scene, object category, or visual theme) and are retained. When SSCD increases, pairs are near-duplicates

Fig. 20 shows five representative clusters detected by SSCD that pHash misses. The image with a green border in each row is the representative kept in the final dataset; the others are discarded. The clusters illustrate the typical failure modes of pHash that SSCD is able to recover: cropping and re-framing of the same scene, watermark or logo overlays, color and exposure adjustments, and partial background edits. Because SSCD operates on

semantic image content rather than raw spatial frequencies, it groups these variants together while remaining selective enough to leave visually distinct images untouched.

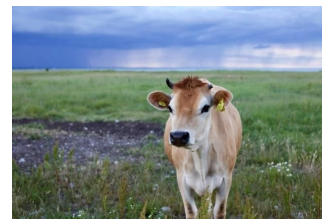
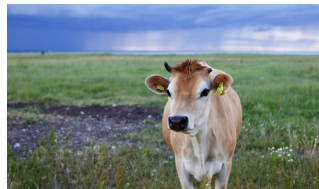
Limitations: false positives on template-based content SS CD embeddings capture mid-level visual structure but are largely insensitive to textual content rendered within images. Fig. 21 illustrates this with two pairs, bar charts and quotes generated from identical templates but reporting entirely unrelated content. SS CD assigns them cosine similarities of 0.92/0.91, well above our 0.75 removal threshold, even though the underlying data and titles differ completely. Discarding such pairs is counterproductive, as they would otherwise help the T2I model learn to render text. Addressing this limitation, *e.g.* through OCR-aware deduplication for text-heavy images or content-aware hashing conditioned on semantic features rather than raw spatial frequencies, is an important direction for future work.



Cluster 1



Cluster 2



Cluster 3

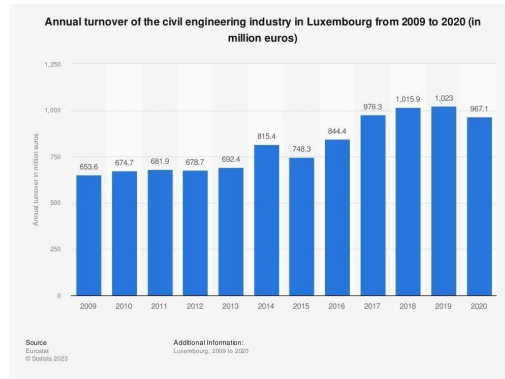
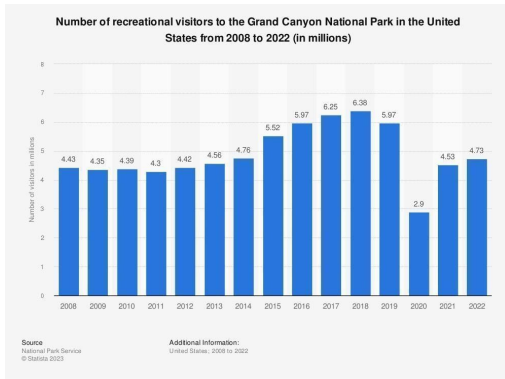


Cluster 4

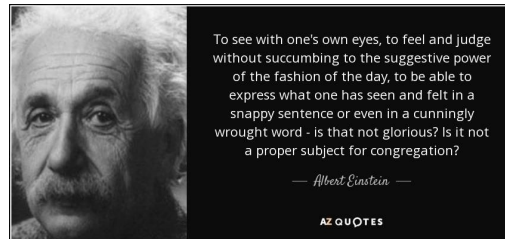
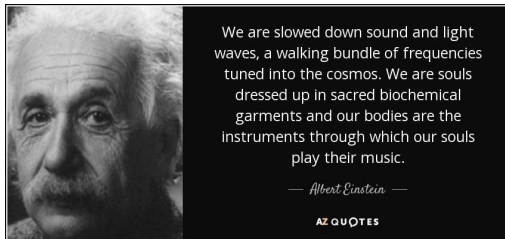


Cluster 5

Figure 20: Examples of near-duplicate clusters detected by SSCD. Each row shows one cluster; the image with a green border is the representative we keep in the dataset, while the remaining images are discarded as duplicates.



SSCD=0.92, $d=20$



SSCD=0.91, $d=4$

Figure 21: SSCD false positives on template-based content. *Top*: two unrelated bar charts sharing the same visual template receive SSCD=0.92 despite completely different data; pHash correctly assigns $d=20$. *Bottom*: two quotes images with identical portrait but different text are flagged by both SSCD (0.91) and pHash ($d=4$).

A.3 Re-captioning with VLMs

A.3.1 Captioning models and prompts

VLM captioners were prompted with minimal, model-appropriate instructions to elicit each model’s default captioning behavior, with no in-context examples or formatting constraints beyond what is noted below. Specifically, **Florence2-large**³ was used in its built-in <DETAILED_CAPTION> mode; **ShareGPT4V**⁴ and **InternVL3-8B**⁵ were prompted with “Describe this image”; and **Gemini 2.5 Flash Lite**⁶ was prompted with “Describe this image in detail. Describe the main objects in the image, their relationships, the scene, the style. The caption should be in the language of the prompt without any line breaks or bullet points.” This minimal prompt design was chosen to enable a fair comparison across captioners, since prompt phrasing can significantly affect output style, length, and content.

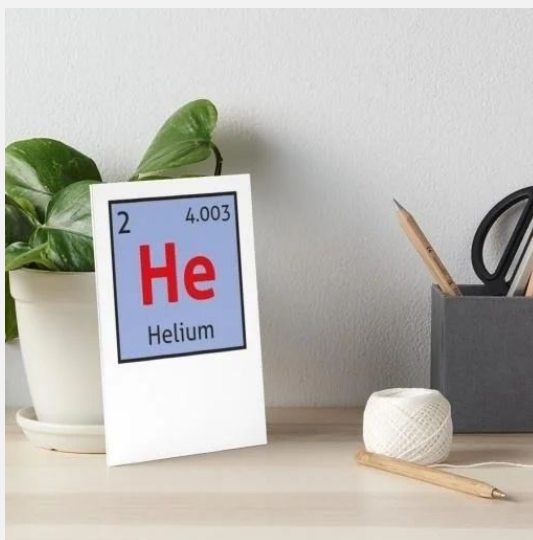
This section complements the main-paper example (Fig. 6) with five additional representative re-captioning examples from MONET, see Figs. 22, 23, 24, 25 and 26. Qualitatively, the **original** web captions are often unreliable, sometimes missing the image content entirely or describing unrelated context. **Florence2** produces the shortest captions while remaining accurate, **ShareGPT4V** and **InternVL3-8B** bring noticeable improvements in coverage and specificity, and **Gemini 2.5 Flash Lite** yields substantially more detailed descriptions of objects, relationships, scene, and style.

³<https://huggingface.co/microsoft/Florence-2-large>

⁴<https://huggingface.co/Lin-Chen/ShareGPT4V-7B>

⁵<https://huggingface.co/OpenGVLab/InternVL3-8B-Instruct>

⁶<https://ai.google.dev/gemini-api/docs/models/gemini-2.5-flash-lite>



Original: The Periodic Table – Helium Art Board Print

Florence: The image shows a desk with a potted plant, a card with the element helium, a thread roll, a pencil, scissors, and a box of pencils placed on it. In the background, there is a wall.

ShareGPT4V: The image captures a serene workspace setup. Dominating the scene is a white desk, which hosts a variety of objects. On the left, a potted plant adds a touch of greenery to the setting. Adjacent to the plant, a white card stands out with its blue background and red text. The card is adorned with the atomic number 2 and the symbol "He" for helium, indicating a scientific theme. In the center of the desk, a gray pencil holder holds a collection of pencils, ready for use.

Gemini 2.5 Flash Lite: A white card with a blue box representing the element Helium from the periodic table stands on a wooden surface. The card shows the atomic number 2, the symbol He in red, the atomic weight 4.003, and the name Helium in black text. To the left of the card, a potted plant with large green leaves is visible. To the right of the card, a grey box holds pencils and scissors, and a spool of white twine and a wooden pencil lie on the surface. The scene is brightly lit with a soft, natural light, creating a clean and organized aesthetic with a touch of science and crafting.

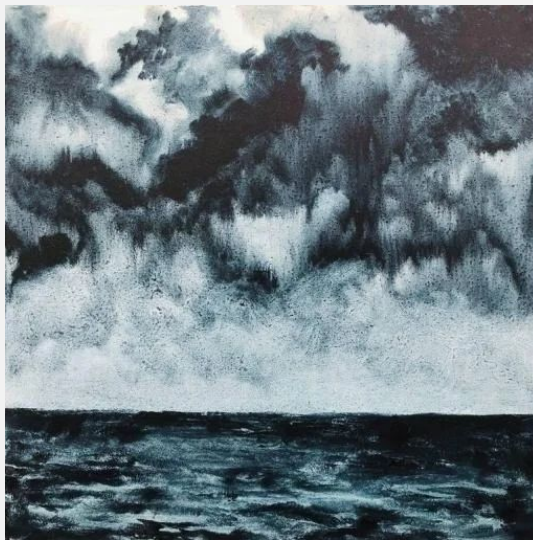
InternVL3-8B: The image shows a desk with a notecard displaying the element helium from the periodic table. Next to the notecard is a potted plant, a container holding pencils and scissors, and a ball of yarn with a needle. The background is a plain wall. The notecard shows features the atomic number, atomic mass, and the chemical symbol and name of the element helium.

Figure 22: Re-captioning example (1/5)

Original: Stormy Seas off the West Coast

Florence: The image shows a black and white painting of a stormy sky over the ocean. The sky is filled with dark, ominous clouds, and the water below is choppy and turbulent.

ShareGPT4V: The image presents an abstract representation of a stormy sea under a dark, cloudy sky. The sea is depicted in a dark blue color, with white waves that add a sense of movement and turbulence. The sky, filled with thick, dark clouds, is rendered in a lighter shade of blue, creating a stark contrast with the sea below. The art style is abstract, characterized by loose brushstrokes that emphasize the interplay of light and shadow. The genre of the artwork is landscape, as it captures the natural elements of the sea and sky.



Gemini 2.5 Flash Lite: This is a monochromatic abstract painting depicting a turbulent sea beneath a dramatic, cloudy sky. The main objects are the sea and the sky, with the horizon line serving as their distinct separation. The sea occupies the lower third of the canvas and is rendered with dark, choppy brushstrokes, suggesting rough waves and an agitated surface. The color is a deep, almost black blue, with lighter tones highlighting the crests and troughs of the waves. Above the sea, the sky dominates the upper two-thirds of the painting. It is filled with swirling, dense clouds rendered in varying shades of dark gray, black, and white. The clouds appear heavy and ominous, with streaks and washes of paint creating a sense of movement and depth, perhaps indicating an approaching storm. The style is abstract and expressive, characterized by a loose, painterly application of pigment. The artist uses a limited palette of blues and grays, and the textured brushwork creates a sense of raw energy and emotion. The overall scene evokes a feeling of atmospheric drama and the power of nature.

InternVL3-8B: The image is a piece of art depicting a seascape under a dramatic sky. The scene shows in the painting predominantly features the ocean and the sky, with dark, heavy clouds suggesting an impending storm. The colors are predominantly shades of dark blue, black, and gray, creating a moody and turbulent atmosphere. The ocean waves are depicted with dynamic brushstrokes, enhancing the sense of movement and unrest in the scene. There is a clear division between the sea and the sky, with the horizon line situated towards the lower third of the composition, emphasizing the vastness of the sky over the sea.

Figure 23: Re-captioning example (2/5)

Original: A baby nurses while dad and brother look on.

Florence: The image shows a man and woman holding a newborn baby in their arms, with a cloth draped over them both. In the background, there are clothes, suggesting that the family is in a room. The man is likely the father, and the woman is likely his wife, as they are both looking lovingly at the baby.

ShareGPT4V: In the image, a family of three is gathered around a baby, creating a warm and intimate atmosphere. The baby, dressed in a white onesie, is the center of attention. The family members, all wearing glasses, are looking down at the baby with expressions of love and affection. The room they are in is dimly lit, adding to the cozy ambiance. The background is filled with clothes, suggesting a home setting. The family's focus on the baby indicates a special moment being shared. The image captures a precious family moment, filled with love and warmth.

Gemini 2.5 Flash Lite: A tender, intimate scene captures a family's love as an older sibling, a young boy, gently holds a newborn baby while their parents look on with affection. The boy, with his dark hair and wide eyes, is dressed in a blue t-shirt and is cradling the infant with one hand, his fingers lightly touching the baby's face. He is nestled against a light blue and white patterned pillow. The baby, swaddled in a pink and white striped blanket and a white cloth, is lying on its back, its head turned towards the viewer. On the left, the father, wearing a striped t-shirt and glasses, leans in, his expression one of gentle observation. On the right, the mother, wearing a black top, looks down at the baby, her face mostly obscured by shadow but her posture radiating care. The overall style of the image is soft and moody, with a shallow depth of field that blurs the background and focuses attention on the family's interaction, creating a warm and emotional atmosphere.

InternVL3-8B: The image shows a family of three, including a baby, gathered closely together. One person, wearing glasses and a striped shirt, is leaning in towards the baby, who is being held by another person in a dark top. The setting appears to be indoors, with soft lighting creating a warm and intimate atmosphere. The family seems to be sharing a tender moment together.



Figure 24: Re-captioning example (3/5)



Original: (PERSON) designed this chess set in 1920 using found objects from his studio. Most of the pieces are geometric models made for still-life drawing (the king is a pyramid, the queen a cone, the rook a cube, the pawn a sphere). (PERSON), Chess Pieces For Sale, Still Life Drawing, Geometric Form, Contemporary Art, Art Pieces, Elegant, King, Lathe

Florence: The image shows a wooden chess board with black and white chess pieces on it, set against a white background. The board is made of wood and the pieces are arranged in a traditional chess formation, with the black pieces on one side and the white pieces on the other.

ShareGPT4V: The image presents a captivating scene of a chess game in progress. The chessboard, with its alternating black and white squares, serves as the stage for this strategic battle. On the black side of the board, there are 12 pieces, each unique in shape and color. They are arranged in a way that suggests a game in progress. The white side of the board is adorned with 11 pieces, mirroring the black side in their arrangement. The pieces on the black side are predominantly black and brown, with a few white and beige ones interspersed.

Gemini 2.5 Flash Lite: A close-up, low-angle shot showcases a modern, minimalist chess set on a wooden chessboard. The board itself is composed of alternating light wood and black squares, with the edges rendered in a natural wood tone. The chess pieces are a striking contrast of matte black and natural, unvarnished wood. The black pieces include a tall, sharp pyramid, several smooth, spherical pawns, a piece resembling a stylized vase with a flat top, and two elaborate, coiling pieces that evoke the form of a scroll or a ram's horn. The wooden pieces are also mostly spherical pawns, with one taller piece shaped like a rounded vase and another a sharp pyramid. The pieces are arranged in a seemingly random, yet strategically suggestive, pattern across the board, hinting at an ongoing game or a unique display. The style is contemporary and abstract, with a focus on geometric shapes and the interplay of light and shadow on the matte surfaces. The overall impression is one of elegant simplicity and artistic design.

InternVL3-8B: The image shows a chess set where the pieces have been replaced with various shapes and forms, yet they retain the original chess piece functions. The board itself features the traditional black and tan squares. Among the pieces, there are black pieces shaped like cones, spheres, and other geometric forms, as well as wooden pieces that resemble spirals, pyramids, and elongated ovals. The modified pieces maintain the classic chess piece roles despite their unconventional appearances.

Figure 25: Re-captioning example (4/5)



Original: Small shopping cart with boxes on top of a laptop keyboard

Florence: The image shows a laptop with a shopping cart filled with cardboard boxes sitting on top of it, suggesting that the laptop is being used to help with e-commerce. The background is slightly blurred, giving the image a sense of focus on the laptop and the cart.

ShareGPT4V: The image presents a scene of online shopping. At the center of the image, a silver shopping cart is filled with three cardboard boxes. The boxes are labeled with the words "FRAGILE", indicating that the items inside are likely delicate and should be handled with care. The cart is placed on a black keyboard, suggesting that the shopping is being done from a computer. To the right of the cart, there's a small cardboard box with the word "FRAGILE" written on it, reinforcing the theme of fragile items.

Gemini 2.5 Flash Lite: A miniature shopping cart, filled with small cardboard boxes, rests on the keyboard of an open laptop. The boxes, with "FRAGILE" printed on them along with shipping symbols, suggest an online shopping or delivery theme. The scene is captured with a shallow depth of field, blurring the background and drawing focus to the main objects. The style is somewhat vintage and warm, possibly achieved through editing filters, evoking a sense of nostalgia or a handcrafted aesthetic.

InternVL3-8B: The image depicts a shopping cart filled with cardboard boxes labeled "FRAGILE." The cart is positioned on top of a laptop keyboard, symbolizing online shopping or delivery services. Additionally, one cardboard box is placed on the laptop's touchpad area, further emphasizing the theme of e-commerce and logistics. The overall scene suggests themes of online purchases, fragility of goods, and possibly the impact on the user experience of shopping from a laptop.

Figure 26: Re-captioning example (4/5)

A.3.2 Human quality assessment

To complement the automatic image–text alignment of Sec. 4, we ran a pairwise human study over 5000 images. Annotators were shown one image and two captions sampled at random among the five captioners (**original**, **Florence2-large**, **ShareGPT4V**, **Gemini 2.5 Flash Lite**, **InternVL3-8B**) with shuffled left/right order, and asked to vote *Neither*, *One is better*, or *Both are good*. Votes were aggregated into a per-captioner Elo score (initialized at 1500, draws for *Both are good*, *Neither* votes discarded). The full instructions provided to annotators are reproduced verbatim below.

Instructions provided to human annotators

In this task, you will be shown **one image alongside two captions**. Your goal is to judge which caption best describes the image. For each pair, select one of:

- **Neither** – neither caption accurately describes the image.
- **One is better** – one caption is clearly more accurate than the other.
- **Both are good** – both captions describe the image equally well.

When making your choice, pay attention to:

- **Accuracy** – does the caption faithfully describe what is visible in the image?
- **Hallucinations** – does it mention elements not present in the image? Be especially careful with longer captions, which may sound detailed but include fabricated content.
- **Completeness** – does it cover the key elements (subject, action, setting)?
- **Specificity** – does it use precise rather than vague or generic language?
- **Objectivity** – does it stick to what is visually observable, without subjective interpretation?

Compensation. Annotators were compensated at \$6/hour, above the average hourly wage of ~\$1.5 in Philippines, the country where the study was conducted. The total budget was capped at \$300 (~50 hours), so the annotators were instructed to stop once their time allowance was reached rather than voting on the full pool. Sign-in was used only to deduplicate votes and was discarded after Elo aggregation.

Cross-encoder alignment with human preferences. Fig. 27 reports the human Elo scores against the cosine similarity of three image–text encoders (**CLIP-L/14-336** [70], **SigLip2** [91] and **Jina-CLIP-v2** [46]) complementing the **LongCLIP** [107] alignment shown in Fig. 7a. **LongCLIP**, **SigLip2** and **Jina-CLIP-v2** are consistent with the human ranking: the longer captions from **Gemini** and **InternVL3-8B** obtain both higher Elo and higher cosine similarity than the **original** and **Florence2** captions, in line with their extended 248-token text context window. We do not draw conclusions from **CLIP-L/14-336**: its 77-token context truncates the long Gemini and ShareGPT4V captions, mechanically capping their similarity and making the metric unreliable for long-form captioners. We therefore recommend long-context encoders such as LongCLIP or Jina-CLIP-v2 for evaluating long-form re-captioning pipelines.

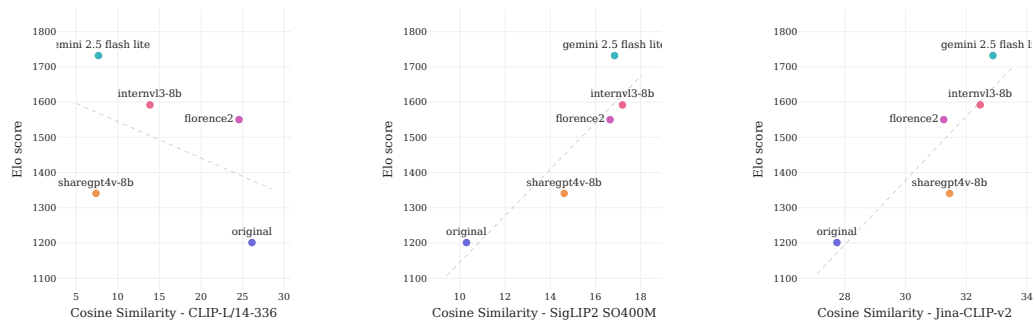


Figure 27: Human Elo scores aggregated from the pairwise voting study, plotted against the cosine similarity computed by CLIP-L/14-336 (left), SigLip2 (middle) and Jina-CLIP-v2 (right). The Elo ranking is consistent with LongCLIP, SigLip2 and Jina-CLIP-v2 cosine similarities, which support long-form captions, but is not well captured by CLIP-L/14-336 due to its 77-token context window, which truncates the long captions produced by Gemini 2.5-Flash-Lite and ShareGPT4V.

A.4 Details on image content and style classifications

A.4.1 Image content distribution

Fig. 28 and 29 show the detailed distribution of MONET’s image content across the three hierarchical levels, using YOLO detection labels and CLIP-based classification, respectively. They show how individual classes are grouped into two higher hierarchy classes to produce the plots of Fig. 8.

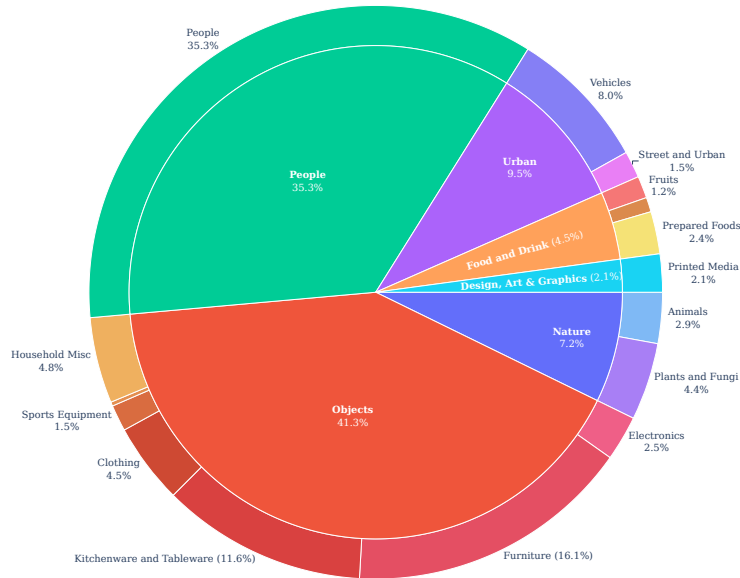


Figure 28: Hierarchical image content distribution (YOLO).

Fig. 30 illustrates successful top-5 CLIP-based classifications on MONET images, demonstrating the model’s ability to retrieve a wide variety of complex concepts using CLIP embeddings. Conversely, Fig. 31 showcases examples where not all top 5 labels are relevant. For instance, in the second image a “machinist” is predicted, while there is no human in the image, and in the third image “arctic animals” are predicted, while there are no visible animals in the picture. On the other hand, the first image depicts a limitation of the hierarchical classification: while predicting “whiskey” is correct, as the infographic is related to whiskeys, the “whiskey” class is later associated to “beverages”, and then to “food and drink”, where the image should belong to “design, art & graphics”. In these failure cases, the top 1 result is frequently a false positive, which justifies our approach of evaluating the top 5 classes rather than relying solely on the top-1 result.

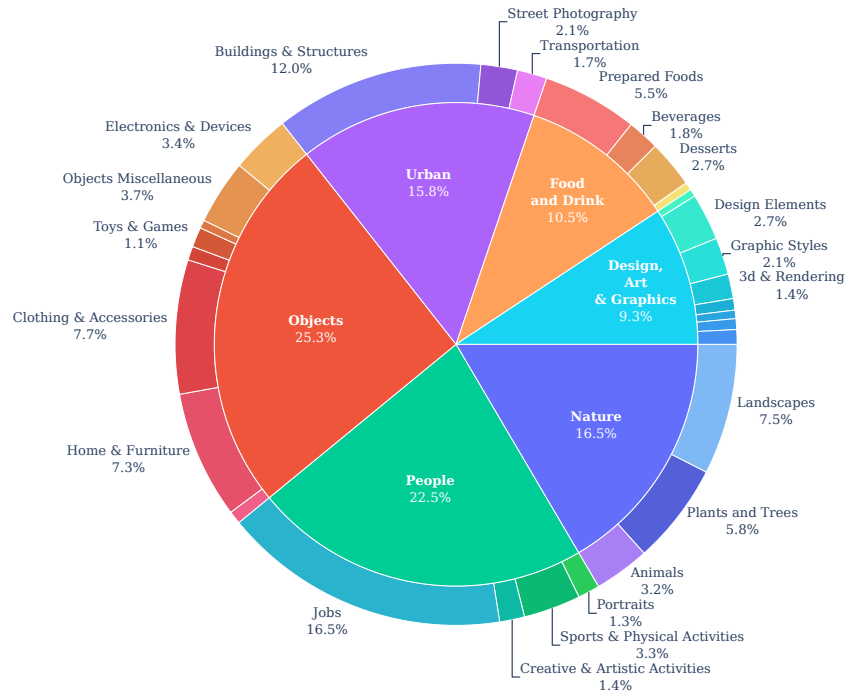


Figure 29: Hierarchical image content distribution (CLIP).

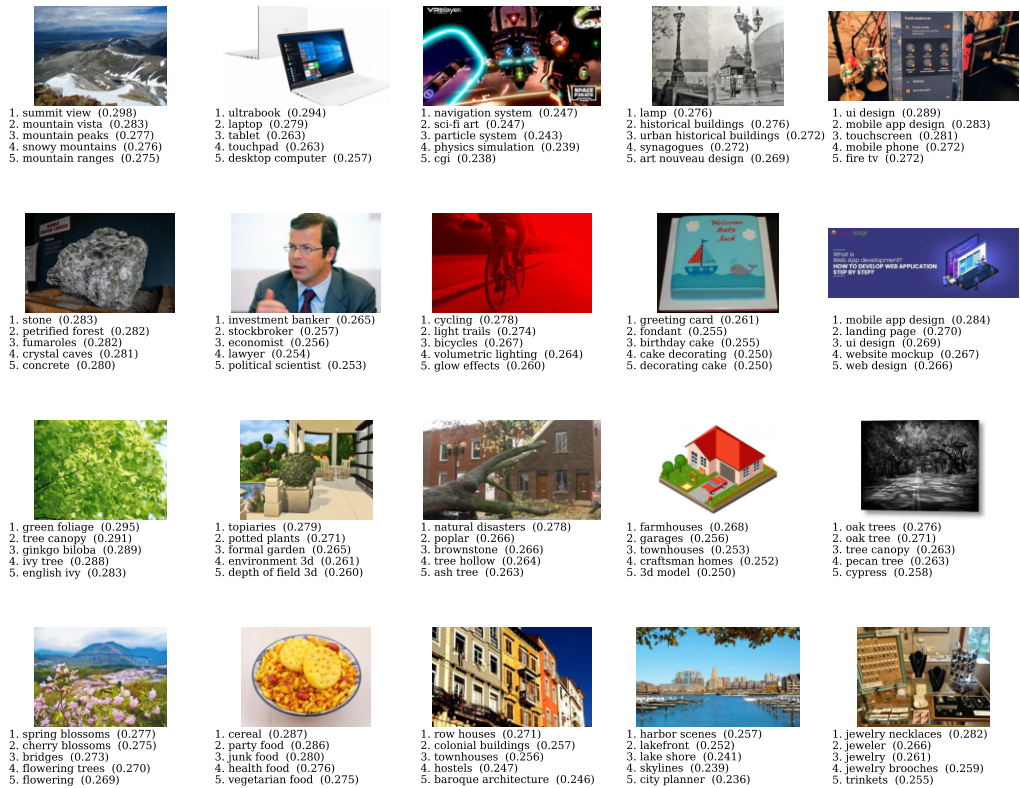


Figure 30: Examples of top 5 image content classification using CLIP with their similarity scores.

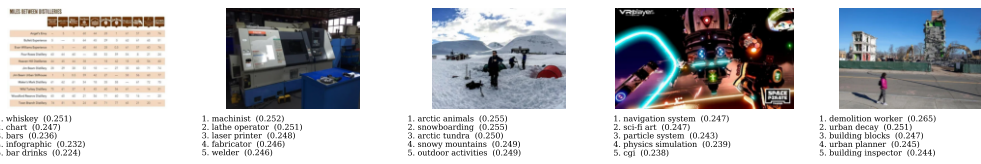


Figure 31: Examples of top-5 image content classifications using CLIP, including some incorrect or misleading classes.

A.4.2 Image style audit prompt and JSON schema

To complement the content distribution above, we annotate every image with a single image style label that captures *how* the image was produced rather than what it depicts. We initially explored CLIP-based zero shot classification for this task, and found that CLIP embeddings were not reliable for distinguishing production-oriented style categories. In particular, they tend to mix visual content with how an image was produced, and they do not consistently capture fine-grained stylistic or medium-related cues. As a result, we process each image using Qwen3-VL-8B-Instruct [105] with the prompt reproduced below, which defines a 15-way taxonomy organised in three families (photography, traditional / digital art, and utility / design) plus an `other` escape hatch. The taxonomy is deliberately production-oriented: photography labels are assigned from visible cues (sensor grain, bokeh, lens geometry, lighting setup) rather than subject matter, so that, for example, a photograph of a painting and the painting itself receive different labels. Fig. 33 illustrates the resulting categories with two representative thumbnails per label sampled from the audit preview, while Fig. 32 reports the full distribution over MONET.

Prompt

Picture-style audit prompt and JSON schema.
A 15-way classification over *how an image was produced*, independent of subject matter. Content classification is handled separately.
The taxonomy is organised in three families: photography, traditional / digital art, and utility / design, with one escape hatch (`other`).

Photography (8)
Always chosen based on *visible production cues* (sensor grain, bokeh, lens geometry, framing, lighting setup), never from the subject alone.

- `portrait_photography` — deliberately posed photographic portrait of a person (studio, editorial, on-location, fashion, beauty, headshot). The person is the intended subject and the shot is directed.
- `product_photography` — commercial still-life of an object or small grouping on a clean or styled background with controlled lighting; e-commerce, packshot, hero shot, food or beauty advertising.
- `monochrome_photography` — any black-and-white, greyscale, or sepia-toned photograph. Monochrome treatment is the defining cue.
- `landscape_photography` — wide-framed colour photograph where the subject is the environment itself: landscape, seascape, cityscape, mountains, forests, deserts, aerial views, astrophotography. People may appear only as scale references.
- `street_photography` — documentary or photojournalistic images of people in public spaces; unposed, observational scenes such as events, protests, or markets.
- `architecture_photography` — deliberate photograph of a building or interior as the primary subject, with strong compositional cues (symmetry, perspective control, wide-angle geometry).
- `wildlife_macro_photography` — photograph of a wild animal, insect, or fine natural detail, with strong telephoto or macro cues (compression, shallow depth of field).
- `casual_photography` — default catch-all for everyday colour photographs: snapshots, selfies, family, travel, food, interiors, social media images.

Traditional / digital art (4)

- `traditional_art` — paintings and classical sculptures, including photographic reproductions of the work itself.
- `anime` — anime or manga-style imagery with cel shading and stylised features.
- `illustration` — non-anime illustration such as concept art, vector graphics, cartoons, comics, pixel art, or digital painting.
- `sketch` — line-based drawings such as pencil, ink, or charcoal sketches, technical drawings, engravings, or woodcuts.

Utility / design (2)

- `3d_render` — computer-generated imagery (photoreal or stylised), including product visualisation, animation stills, and game renders.

- `graphic_design` — posters, advertisements, layouts, infographics, typography-heavy designs, UI screenshots, or documents.

Escape hatch

- `other` — anything that does not fit the above categories.

A.4.3 Image style distribution

Fig. 32 shows the detailed distribution of image styles, as in Fig 8 (right) classes with less than 2% representation were grouped in the “other” class. We highlight the high variability of image styles in the dataset. Fig. 33 shows two examples per image style category, illustrating that the VLM-based image style classification (e.g., sketch, illustration, etc.) is consistent and reliable.

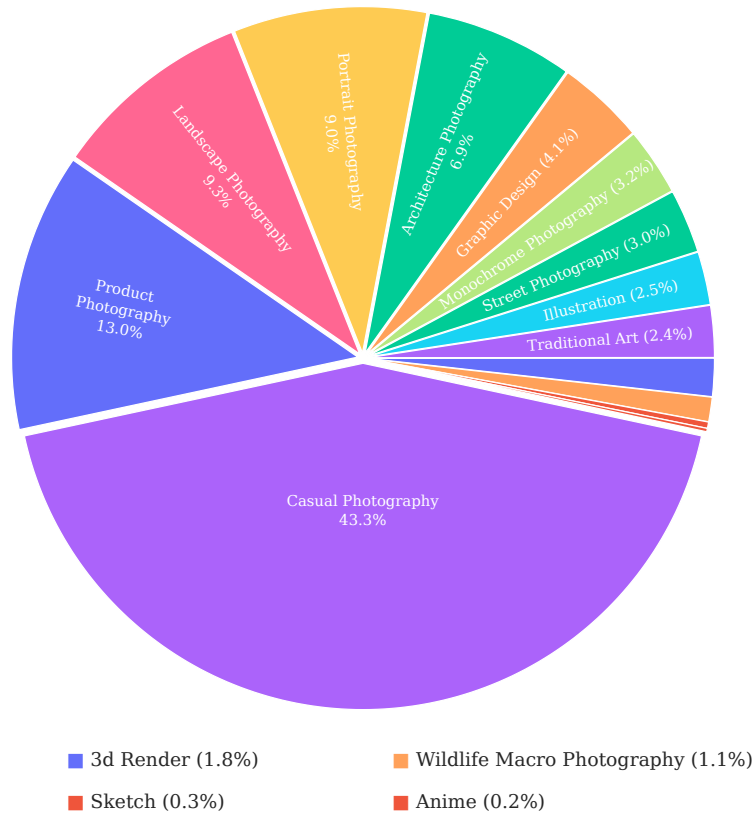


Figure 32: Detailed image style distribution.

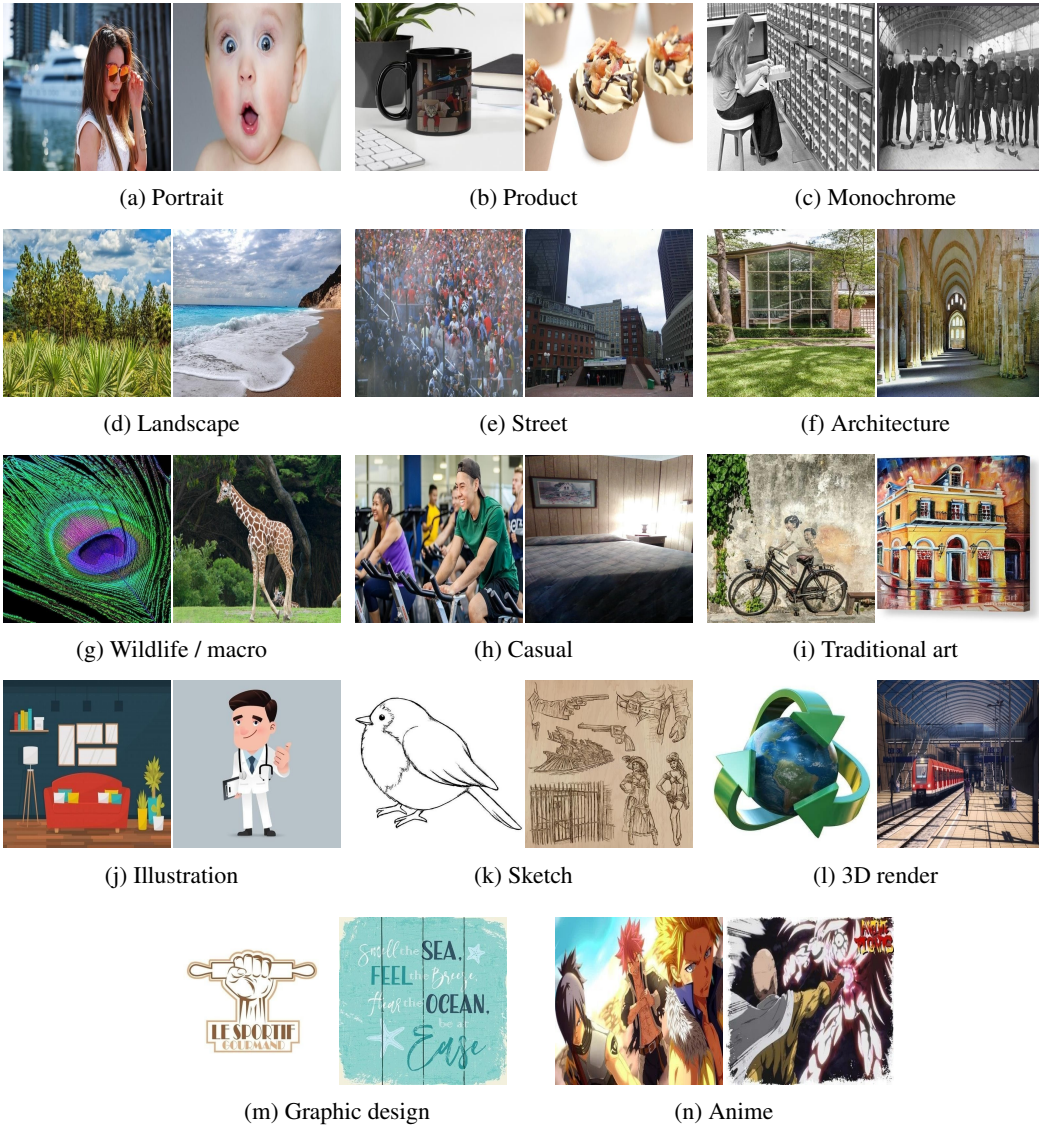


Figure 33: Example images per picture-style label sampled from the audit preview.

A.5 Training details

Captioning models and synthetic data ablations For these ablations, we trained the models on images of resolution 512×512 for 400k iterations on 2 H200 GPUs, using 16 dual-stream MMDiT blocks [19] with 24 attention heads of size 128. The text conditioning is passed either through the Qwen3-4b pre-trained Large Language Model (LLM) [105] (for the synthetic data ablation) or T5 [71] (for the captioner ablation). The output of the antepenultimate layer (Qwen3-4b) or the last layer (T5) serves as conditioning for the denoiser. While training the model, as is standard practice, we also replace the text conditioning with an empty prompt "" 10% of the time allowing to perform Classifier-free guidance [31] at inference time. We relied on the Latent Diffusion Model framework [76] to train our models using the SANA1.5 VAE model [102] which spatially compresses an input image by a factor of 32 and used the flow matching approach [58, 60]. Metrics are computed using samples generated with 50 denoising steps and a guidance scale of 5. All training images are resized to 512×512 and we trained the model with a global batch size of 512, using a learning rate of $1e^{-4}$ together with AdamW optimizer [45].

T2I model training details When training our 4 billion parameters T2I model, we relied on a denoiser combining 32 MMDiT blocks [19] mixing single (16) and dual stream blocks (16) all with 20 attention heads of size 128. The text conditioning is passed through the Qwen3-4b pre-trained Large Language Model (LLM). The output of the antepenultimate layer of the text encoder serves as conditioning for the denoiser. While training the model, as is standard practice, we also replace the text conditioning with an empty prompt "" 10% of the time allowing to perform Classifier-free guidance at inference time. We relied on the pre-trained Deep Compression VAE from SANA1.5 model. We employed a multi-stage approach for training the model using the findings exposed in the previous sections. We directly started training the model on 512×512 images using 75% of synthetic data and the most verbose captioners namely *gemini-2.5-flash-lite* (50%) and *internvl3-8b* (50%). We then progressively reduce the amount of synthetic data to 50% and 30%. We then increase the resolution of the images to 1024×1024 and progressively include the other captioners such that they are equally represented in the final training dataset as described in Table 4. The model was trained relying on the flow matching approach [58, 60] and optimized using the AdamW optimizer [45].

Table 4: 4B parameters text-to-image model training details used for the benchmarks.

	Res.	Batch size	Learning rate	H200 GPUS	Steps
Phase 1	512	256	$1e^{-4}$	16	350,000
Phase 2	512	1536	$3e^{-5}$	24	420,000
Phase 3	512	3072	$1e^{-5}$	16	45,000
Phase 4	1024	256	$1e^{-5}$	16	35,000

A.6 Additional results

A.6.1 Quantitative results

We provide in Table 5 and Table 6 additional comparisons on the GenEval and DPG benchmarks [25, 37], which assess short and dense prompt-following capabilities across multiple semantic categories. The tables report quantitative results with our model trained on the fully open MONET dataset against *state-of-the-art* text-to-image models trained on closed-source data. Despite relying solely on open data, our 4B model achieves a competitive overall score of 0.74 on GenEval and 85.56 on DPG, outperforming several strong baselines, including FLUX.1 [Dev], SD3 Medium, and Janus-Pro-7B. It nonetheless underperforms on the *other* category of DPG, which assesses among others the capacity of the model to write text on an image. Since MONET does not contain much of this type of text-image pairs, the model is unable to generate faithful text rendering. Existing datasets specifically design for such use cases can be used for further finetuning and enriching our MONET dataset that was mainly design for pre-training purposes.

Table 5: GenEval benchmark. Our 4B model trained specifically on the fully open MONET dataset is able to compete with many existing text-to-image models which were trained on closed-source data.

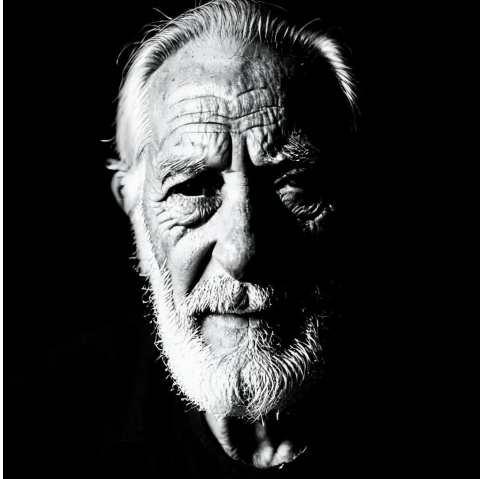
Model	Params. (B)	Objects		Counting	Colors	Position	Color	Overall \uparrow
		Single	Two					
SD v1.5 [76]	0.9	0.97	0.38	0.35	0.76	0.04	0.06	0.43
PixArt- α [10]	0.6	0.98	0.50	0.44	0.80	0.08	0.07	0.48
SD v2.1 [76]	0.9	0.98	0.51	0.44	0.85	0.07	0.17	0.50
DALL-E 2 [73]	3.5	0.94	0.66	0.49	0.77	0.10	0.19	0.52
Show-o [103]	1.3	0.95	0.52	0.49	0.82	0.11	0.28	0.53
Emu3-Gen [96]	8.0	0.98	0.71	0.34	0.81	0.17	0.21	0.54
SDXL [68]	2.6	0.98	0.74	0.39	0.85	0.15	0.23	0.55
SDXL Turbo [80]	2.6	1.00	0.72	0.49	0.80	0.10	0.18	0.55
SD3 Medium [19]	2.0	0.98	0.74	0.63	0.67	0.34	0.36	0.62
JanusFlow [62]	1.3	0.97	0.59	0.45	0.83	0.53	0.42	0.63
FLUX.1 [Dev] [48]	12.0	0.98	0.81	0.74	0.79	0.22	0.45	0.66
DALL-E 3 [3]	-	0.96	0.87	0.47	0.83	0.43	0.45	0.67
SD3.5 Large [19]	8.0	0.98	0.89	0.73	0.83	0.34	0.47	0.71
SANA-1.5 [102]	4.8	0.99	0.85	0.77	0.87	0.34	0.54	0.72
Lumina-Image 2.0 [69]	2.0	-	0.87	0.67	-	-	0.62	0.73
Janus-Pro-7B [14]	7.0	0.99	0.89	0.59	0.90	0.79	0.66	0.80
HiDream-I1-Full [7]	17.0	1.00	0.98	0.79	0.91	0.60	0.72	0.83
GPT Image 1 [63]	-	0.99	0.92	0.85	0.92	0.75	0.61	0.84
Seedream 3.0 [23]	-	0.99	0.96	0.91	0.93	0.47	0.80	0.84
Z-Image [106]	6.0	1.00	0.94	0.78	0.93	0.62	0.77	0.84
Qwen-Image [97]	20.0	0.99	0.92	0.89	0.88	0.76	0.77	0.87
Ours	4.1	1.00	0.90	0.73	0.88	0.35	0.62	0.74

Table 6: Quantitative evaluation results on DPG. Our 4B model trained on the fully open MONET dataset achieves competitive performance against models trained on closed-source data.

Model	Params. (B)	Global	Entity	Attribute	Relation	Other	Overall \uparrow
SD v1.5 [76]	0.9	74.63	74.23	75.39	73.49	67.81	63.18
PixArt- α [10]	0.6	74.97	79.32	78.60	82.57	76.96	71.11
Lumina-Next [113]	2.0	82.82	88.65	86.44	80.53	81.82	74.63
SDXL [68]	2.6	83.27	82.43	80.91	86.76	80.41	74.65
Playground v2.5 [53]	2.6	83.06	82.59	81.20	84.08	83.50	75.47
Hunyuan-DiT [56]	1.5	84.59	80.59	88.01	74.36	86.41	78.87
Janus [98]	1.3	82.33	87.38	87.70	85.46	86.41	79.68
PixArt- Σ [11]	0.6	86.89	82.89	88.94	86.59	87.68	80.54
Emu3-Gen [96]	8.0	85.21	86.68	86.84	90.22	83.15	80.60
Janus-Pro-1B [14]	1.0	87.58	88.63	88.17	88.98	88.30	82.63
DALL-E 3 [3]	-	90.97	89.61	88.39	90.58	89.83	83.50
FLUX.1 [Dev] [48]	12.0	74.35	90.00	88.96	90.87	88.33	83.84
SD3 Medium [19]	2.0	87.90	91.01	88.83	80.70	88.68	84.08
Janus-Pro-7B [14]	7.0	86.90	88.90	89.40	89.32	89.48	84.19
GPT Image 1 [63]	-	88.89	88.94	89.84	92.63	90.96	85.15
HiDream-I1-Full [7]	17.0	76.44	90.22	89.48	93.74	91.83	85.89
Lumina-Image 2.0 [69]	2.0	-	91.97	90.20	94.85	-	87.20
Z-Image [106]	6.0	93.39	91.22	93.16	92.22	91.52	88.14
Seedream 3.0 [23]	-	94.31	92.65	91.36	92.78	88.24	88.27
Qwen-Image [97]	20.0	91.32	91.56	92.02	94.31	92.73	88.32
Ours - 4B	4.1	84.80	91.76	89.70	94.16	79.60	85.56

A.6.2 Generation examples

This section complements the main-paper qualitative samples (Fig. 11) with additional generations from our 4B T2I model *exclusively* trained on the MONET dataset. Figs. 34 and 35 show additional 1024×1024 samples spanning a variety of artistic styles, while Figs. 37 and 36 report 2048×2048 samples. The model is able to generate high quality images of different styles with strong prompt alignment, showcasing the diversity of the MONET dataset and the quality of its captions, and highlighting that its strong aesthetic supports training even beyond the standard 1024 resolution.



A moody black and white film portrait of an older artisan. The lighting is extremely dramatic high-key chiaroscuro, illuminating only one half of the face in sharp relief, casting the rest into deep, absolute shadow. The texture of their wrinkles and beard is hyper-detailed. Grainy analog film aesthetic.



A raccoon trapped inside a glass jar full of colorful candies, the background is steamy with vivid colors.



A whimsical purple and pink dragon made of clay, showing tiny fingerprint marks and handcrafted texture, soft studio lighting, stop-motion aesthetic.



Professional product photography of a glass skin-care bottle on a floating stone plinth. Surround the bottle with clean, splash-frozen water droplets. Pure white background, studio lighting, sharp focus on the glass texture.

Figure 34: Generation from our 4B model (1024 × 1024) showcasing its ability to generate high resolution images thanks to the MONET Dataset.



A portrait of an old man with his eyes closed and a blue jacket. He is wearing a yellow cap with a purple square on it and red glasses.



A dynamic street scene of Tokyo reimagined entirely as an abstract expressionist oil painting. The image must have violent, thick, impasto brushstrokes of primary colors (red, yellow, blue, black) applied messily and dynamically with a palette knife on raw canvas. Show the extreme texture of the paint.



A vibrant pointillist painting of a garden in Paris. The entire scene is composed of millions of tiny, precise, distinct dots of pure, unmixed color that blend optically.



A luminous aquarelle painting of a misty Venice canal. The style emphasizes translucent washes of paint, soft blending edges, and visible bleeding. The texture of the textured watercolor paper is prominent, and the light passes through the paint.

Figure 35: Generation from our 4B model (1024×1024) showcasing its ability to generate images with different styles thanks to the MONET Dataset.



A detailed portrait of a person with distinctive red, wavy hair stands out, wearing a blue garment with a black ribbon tied at the collar over a white undergarment. They are also adorned with a fur cloak featuring a pattern of black spots, giving the scene a historical or classical atmosphere.



A stunningly detailed, wide-aperture macro shot of a colorful parrot. The focus is tack-sharp on the eye and the tiny, fine feathers of the face. The background is a velvety, pitch-black absorption. Natural, soft-box lighting reveals the organic textures of the beak, including tiny scratches and natural imperfections. The feathers transition from fiery orange to deep violet with a soft, downy texture visible at the neck.



Colossal obsidian wave cresting under a star-drenched indigo sky, framing a gargantuan violet planet. Ethereal purple moonlight illuminates churning sea foam and translucent water, creating a cinematic, hyper-realistic cosmic landscape.

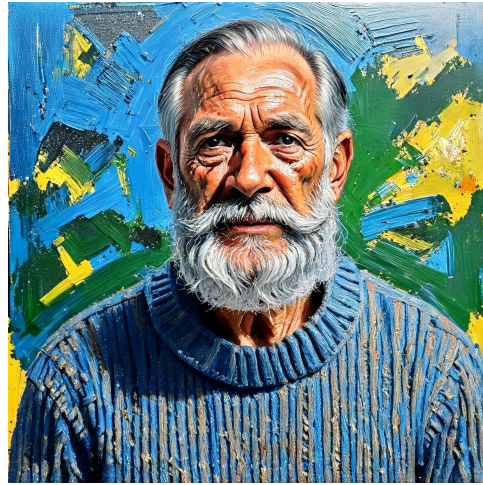


The image shows a very old man with white hair and a white beard. He is wearing a red shirt and blue pants in front of a big green tree and a lake covered with snow.

Figure 36: 2048 × 2048 generation from our 4B model.



An ultra-detailed nocturnal landscape of a hidden tropical lagoon. The water glows with intense neon blue bioluminescence where it laps against jet-black volcanic sand. Towering ancient banyan trees with glowing hanging vines frame the scene. In the background, a massive silver moon hangs low over a calm ocean, casting a shimmering path on the waves. Fireflies create bokeh light clusters in the dark jungle shadows. Intricate textures of wet sand and leaf veins. Surreal atmospheric lighting, high contrast, 16k masterwork, Unreal Engine 5 render style.



A rugged, textured oil painting portrait of an older, weathered fisherman with a thick grey beard and ruddy, sun-exposed skin. He is looking directly at the viewer. He wears a heavy, chunky knit sweater in blues and greys. The entire image is composed of very thick, visible, expressionistic impasto brushstrokes. The background is an abstract blend of choppy blues, greens, and yellows, rendered with dynamic, loose paint application. Raw texture, vivid color palette.

Figure 37: 2048 × 2048 generation from our 4B model.

A.7 Ethics audit

We audit a random sample of 5M images from MONET using Qwen3-VL-8B-Instruct with the structured prompt detailed in Fig. A.7. The model generates an unconstrained JSON response that is then parsed and normalized into our annotation taxonomy. The prompt enforces a chain-of-thought annotation protocol: the model must ground every label in concrete visual evidence and default to "unknown" or "none" when evidence is insufficient. Fig. 38 provides an aggregated view of the results from this audit across twelve dimensions: *cultural origin*, *region*, *Fitzpatrick skin tone* (1–6 [21]), *predominant gender*, *predominant age*, *people count*, *identifiable faces*, *stereotypical depiction*, *prototypicality bias*, *body diversity*, *socioeconomic signal*, and *power dynamics*. Cultural origin and region are dominated by European and North American contexts, consistent with the Western bias of Common-Crawl-derived corpora [82]. Skin tones concentrate around categories 3–4, with both lighter (1–2) and darker (5–6) tones under-represented. Gender is roughly balanced between masculine and feminine-presenting subjects, while age skews strongly toward adults, with children, teenagers and elderly subjects less frequent. Most images contain no people; when people are present, body diversity skews toward *average*, socioeconomic cues toward *neutral*, and power dynamics toward *equal* or *neutral*. Identifiable faces, stereotypical depictions and prototypicality bias remain rare in absolute terms. These biases are largely inherited from the upstream web sources, and if this classification was done at the full scale, this should help to re-weight the dataset toward a more balanced distribution.

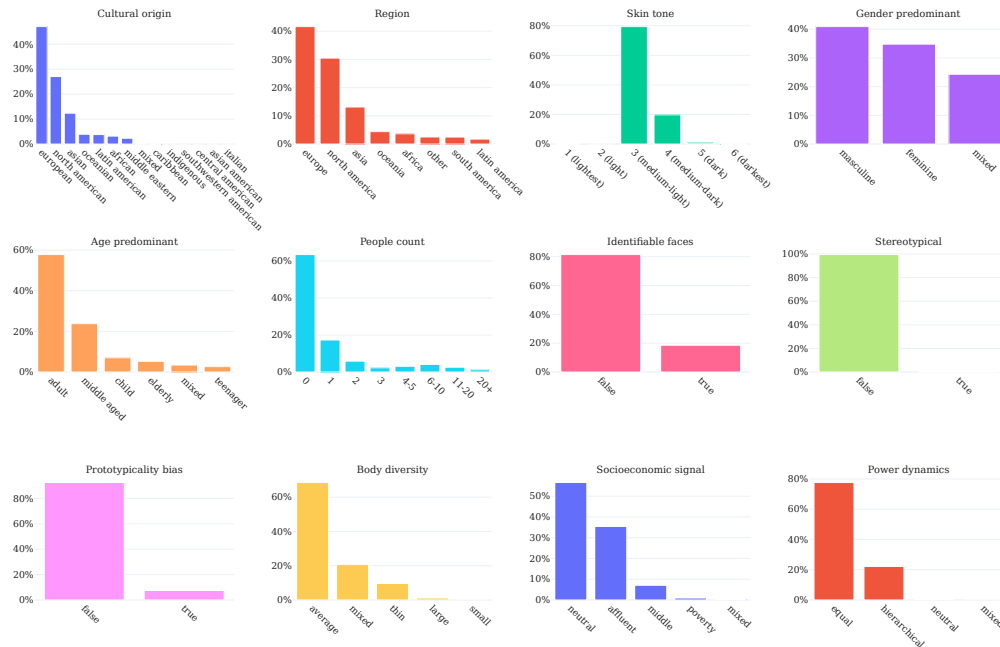


Figure 38: Aggregate distributions from the VLM-based ethics audit over twelve dimensions: cultural origin, region, Fitzpatrick skin tone, predominant gender, predominant age, people count, identifiable faces, stereotypical depiction, prototypicality bias, body diversity, socioeconomic signal, and power dynamics.

Ethics audit prompt

Ethics, representation, and cultural fidelity audit prompt and JSON schema.

A multi-field annotation protocol over *visual evidence of who, where, and how* an image depicts people, places, and cultures. The auditor must ground every label in concrete cues and default to "unknown" or "none" when evidence is insufficient, never inferring culture from surface-level signals (e.g. colour palettes) alone.

System instruction

You are an expert dataset auditor performing a rigorous ethics, representation, and cultural fidelity analysis.

Analyse this image and return a JSON object. Follow a Chain-of-Thought approach: mentally identify specific visual evidence before selecting enums. Do not use surface-level signals (e.g., colour palettes) to infer culture; look for localised attire, vernacular architecture, or distinct signage. If something is not determinable, use "unknown" or "none". Do not hallucinate — only report what is clearly visible.

Demographics and people

- `people_count` — integer count of visible people.
- `demographics` — predominant gender (masculine, feminine, mixed), predominant age (child, teenager, adult, middle-aged, elderly, mixed), mean Fitzpatrick skin tone [21] (1–6 or unknown), and body diversity (thin, average, large, small, mixed).

Place and culture

- `geography` — region (europe, north america, asia, oceania, africa, south america, latin america, other).
- `cultural_depth` — cultural origin (european, north american, asian, oceanian, latin american, african, middle eastern, caribbean, indigenous, southwestern american, central american, asian american, italian, mixed).

Scene and framing

- `social_dynamics` — power dynamics (equal, hierarchical, neutral, mixed) and socioeconomic signal (neutral, affluent, middle, poverty, mixed).

Ethical flags and metadata

- `ethical_flags` — stereotypical depiction and prototypicality bias (boolean).
- `image_metadata` — identifiable faces (boolean).

Key annotation rules

- Geography is inferred only from strong visual evidence, defaulting to "unknown" to avoid hallucinated Western-centric priors.
- `power_dynamics` is set to "hierarchical" only when framing or positioning implies authority/subordination (e.g. "white saviour" compositions).
- `prototypicality_bias` flags images that default to canonical Western stereotypes despite a different semantic context.

A.8 Datasheet

We provide a datasheet for MONET following the template of Gebru et al. [24]. References to other appendices and to the main paper are given where the relevant material is described in more detail.

A.8.1 Motivation

For what purpose was the dataset created? MONET was created to fill the gap of *open-source, filtered, deduplicated* and *recaptioned* image–text datasets suitable for pre-training large text-to-image (T2I) models (Sec. 1). Existing public datasets at this scale (e.g. LAION-400M/5B, COYO) are uncurated, contain large amounts of redundant and low-quality content, and ship with short alt-text captions that limit the performance of modern T2I models. MONET addresses these issues by combining nine heterogeneous open sources (6 *real* and 3 *synthetic*), applying rigorous safety, deduplication and domain-based filtering, and providing multi-model synthetic captions of varying complexity.

Who created the dataset (e.g., which team, research group) and on behalf of which entity (e.g., company, institution, organization)? The dataset was created by the authors of this paper at Jasper Research.

Who funded the creation of the dataset? If there is an associated grant, please provide the name of the grantor and the grant name and number. Creation of the dataset was funded by Jasper Research. No external grant is associated with this work.

Any other comments? None.

A.8.2 Composition

What do the instances that comprise the dataset represent (e.g., documents, photos, people, countries)? Each instance is an image paired with one or more textual captions and a rich set of structured metadata (embeddings, detection and classification outputs, pre-computed VAE latents, and provenance/licensing information).

How many instances are there in total (of each type, if appropriate)? MONET contains **104.9M** image–text pairs in total. Of these, $\sim 91\text{M}$ are real images sourced from six open datasets: 46.6M from LAION-2B-en, 19.1M from COYO, 11.2M from Common-Catalog-CC-BY, 8.0M from Megalith-10M, 6.4M from Conceptual-12M, 12.8k from Diffusion-Aesthetic-4K. And $\sim 13.8\text{M}$ are synthetic images generated in-house: 5.9M from Z-Image, 4.4M from FLUX.1-schnell, and 3.5M from FLUX.2-klein-4B. Per-source counts are reported in Table 1.

Does the dataset contain all possible instances or is it a sample (not necessarily random) of instances from a larger set? MONET is a heavily filtered sample of a much larger pool: starting from $\sim 2.9\text{B}$ raw image–text pairs across the six real sources, the curation pipeline (Sec. 3) yields the final 104.9M pool. The sample is therefore not representative of the original web distribution: it is biased toward higher-aesthetic, higher-resolution, deduplicated and safety-filtered content.

What data does each instance consist of? Each instance contains: (i) the original image (URL pointer to the upstream source); (ii) the original caption(s); (iii) up to four synthetic captions from Florence2 [100], ShareGPT-4v [13], InternVL3-8B [112], and Gemini-2.5-flash-lite [15]; (iv) DINOv2 [64], CLIP [70] and SSCD [66] embeddings; (v) YOLO-v9e object-detection boxes (80 COCO categories), YOLO-v8x ImageNet-1k classification scores, and MediaPipe [61] face counts/boxes/landmarks; (vi) a pre-encoded SANA-VAE [102] latent; (vii) aesthetic score, perceptual hash, and source/license metadata. We also release an index from all vector embeddings for efficient nearest-neighbor search and analysis.

Is there a label or target associated with each instance? The captions act as the natural target for T2I training. Beyond captions, the dataset ships dense per-image annotations (object detections, ImageNet-1k class distribution, face metadata, embeddings, aesthetic scores) usable as labels for retrieval, classification and conditional-generation tasks.

Is any information missing from individual instances? A small fraction of instances may be missing some derived fields (e.g., failed VLM caption generations, undetected faces, or skipped ethics-audit and image-style annotations, the latter of which are computed only on subsets). Original alt-text may be missing or empty for a subset of upstream instances. Original image URLs may also become unreachable over time due to URL rot, although image bytes themselves are preserved in the release.

Are relationships between individual instances made explicit (e.g., users’ movie ratings, social network links)? Explicit relationships are not annotated, but near-duplicate links are implicitly available via the released SSCD embeddings and the accompanying nearest-neighbor index. The source/provenance metadata also groups instances by upstream dataset.

Are there recommended data splits (e.g., training, development/validation, testing)? MONET is intended primarily for unsupervised T2I pre-training and is released as a single pool without official train/val/test splits. Users should hold out their own evaluation sets and avoid contamination with their downstream benchmarks. We leave for future work the creation of specific subsets such as high-resolution, or style-specific subsets.

Are there any errors, sources of noise, or redundancies in the dataset? Synthetic captions are model-generated and may occasionally hallucinate details; we mitigate this by providing captions from multiple captioners with different biases and complexities (Sec. 3.6). Aesthetic scores, NSFW classifier outputs, watermark probabilities, ethics-audit labels and image-style labels are all model-inferred and not human-verified at scale. Despite SSCD-based near-duplicate removal, residual semantic redundancy remains by design (we keep visually distinct but semantically related images, e.g. different frames from the same series).

Is the dataset self-contained, or does it link to or otherwise rely on external resources (e.g., websites, tweets, other datasets)? The dataset is self-contained: all image bytes, embeddings, captions, detections, VAE latents, and metadata are directly included and hosted as part of the release. Upstream image URLs are also kept for each entry to enable cross-referencing and provenance tracking, but all content necessary to use, reproduce, or analyze the dataset is available locally and does not require access to any external resources. URL rot is acknowledged as a limitation affecting URL fields, but it does not affect dataset completeness or usability, as the primary data (images, metadata, and features) are preserved within the release.

Does the dataset contain data that might be considered confidential (e.g., data that is protected by legal privilege or by doctor-patient confidentiality, data that includes the content of individuals’ non-public communications)? No. All instances originate from publicly available web sources or are synthetically generated; the dataset contains no privileged, doctor-patient, or non-public-communications content. As a source-governance measure, domain-based filtering excludes URLs from a blocklist of known stock-photo providers (e.g., Getty Images, Unsplash, Dreamstime, Shutterstock); this is an exclusion control rather than a representation of legal clearance, and residual items flagged by users will be removed upon request.

Does the dataset contain data that, if viewed directly, might be offensive, insulting, threatening, or might otherwise cause anxiety? The corpus is sourced primarily from Common-Crawl-derived datasets and, despite our best efforts at filtering, may still contain offensive, distressing, or otherwise objectionable content. We did our best to mitigate such content by applying multiple safety layers: CSAM removal via the vetted Re-LAION-2B-en-safe annotations, NSFW filtering with an ensemble of three classifiers (Falcon, Bumble, internal) under a union rule, and a DINOv2 nearest-neighbor audit (Sec. 3.3).

Does the dataset identify any subpopulations (e.g., by age, gender)? Sub-populations are identified at the *image level* via the VLM-inferred ethics-audit fields (gender counts, age counts, skin-tone, geographic/cultural origin). Distributions reveal a Western bias inherited from web sources: cultural origin is dominated by European and North American contexts, skin tones concentrate around Fitzpatrick categories 3-4, gender is roughly balanced, and age skews toward adults (Sec. 6). These annotations are coarse, model-inferred, and intended for dataset-level statistics not as ground truth for individuals.

Is it possible to identify individuals (i.e., one or more natural persons), either directly or indirectly (i.e., in combination with other data) from the dataset? The dataset contains naturally occurring web images that may include identifiable people. We do not perform face blurring. We release MediaPipe face counts/boxes/landmarks so that downstream users can implement privacy-aware subsampling or blurring as needed. Individuals seeking removal can contact the maintainers.

Does the dataset contain data that might be considered sensitive in any way (e.g., data that reveals racial or ethnic origins, sexual orientations, religious beliefs, political opinions or union memberships, or locations; financial or health data; biometric or genetic data; forms of government identification, such as social security numbers; criminal history)? As a web-scraped corpus, MONET may incidentally contain images depicting religious symbols, political imagery, locations, or other content from which sensitive attributes could be inferred. We do not deliberately collect or annotate such attributes, and we do not include any government-identification, financial, health, biometric template, or criminal-history data. Coarse, model-inferred demographic statistics (gender, age, skin-tone, geographic/cultural origin) are released for dataset-level auditing only and should not be used to infer sensitive attributes about individuals.

Any other comments? None.

A.8.3 Collection Process

How was the data associated with each instance acquired? Image-text pairs are not collected directly; they are inherited from existing open-source datasets (Sec. 3, Table 1). LAION-2B-en and COYO scrape Common Crawl alt-text; Common-Catalog-CC-BY uses Flickr (YFCC100M) images recaptioned with BLIP2; Megalith-10M is sourced from Flickr; Conceptual-12M crawls the web for alt-text pairs; Diffusion-Aesthetic-4K is a high-resolution web set with GPT-4o captions. Synthetic images and captions are generated in-house with *Apache-2.0* generators (FLUX.1-schnell, FLUX.2-klein-4B, Z-Image) and Qwen3-4B prompt upsampling.

What mechanisms or procedures were used to collect the data (e.g., hardware apparatuses or sensors, manual human curation, software programs, software APIs)? Upstream datasets were downloaded from their public release endpoints using the open-source `img2dataset` downloader and the Hugging Face Hub APIs. All subsequent processing was performed in-house on a GPU cluster of 60 NVIDIA L40S and 80 NVIDIA H200 GPUs ($\sim 175k$ GPU hours in total).

If the dataset is a sample from a larger set, what was the sampling strategy (e.g., deterministic, probabilistic with specific sampling probabilities)? The strategy is filter-based rather than random: each instance is retained if it satisfies all deterministic thresholds of the curation pipeline; no probabilistic subsampling is applied.

Who was involved in the data collection process (e.g., students, crowdworkers, contractors) and how were they compensated (e.g., how much were crowdworkers paid)? The authors (full-time Jasper Research employees) performed all in-house engineering, curation and analysis work as part of their regular employment. The only human-in-the-loop step is small-scale Elo voting on captions performed by a small team of ~ 10 annotators.

Over what timeframe was the data collected? Upstream datasets were downloaded from their public releases between 2022 and 2025. The full curation pipeline ran over a few months of wall-clock time on the in-house cluster.

Were any ethical review processes conducted (e.g., by an institutional review board)? No formal IRB review was conducted, as the dataset is built from already-public web corpora and contains no newly collected human-subjects data.

Did you collect the data from the individuals in question directly, or obtain it via third parties or other sources (e.g., websites)? Indirectly. All images and original captions originate from third-party web corpora; we did not interact with depicted individuals.

Were the individuals in question notified about the data collection? Not by us. Notification, if any, was the responsibility of the upstream dataset providers and original web hosts.

Did the individuals in question consent to the collection and use of their data? Consent was not collected by us. Images were originally posted to public web pages and incorporated into upstream datasets under their respective licenses (CC-BY-4.0, MIT, or equivalent permissive terms).

If consent was obtained, were the consenting individuals provided with a mechanism to revoke their consent in the future or for certain uses? Consent was not obtained directly. Individuals depicted in MONET who wish to have content related to them removed can contact the maintainers (see Maintenance below); we will honor reasonable removal requests in subsequent dataset versions.

Has an analysis of the potential impact of the dataset and its use on data subjects (e.g., a data protection impact analysis) been conducted? Yes. Sec. 6 reports the representation audit on a 5M random sample, characterizing demographic skew. Documented risks and mitigations are summarized in the Responsible Use paragraph of Sec. 6 and the Limitations section (Sec. 7).

Any other comments? None.

A.8.4 Preprocessing, Cleaning, and Labeling

Was any preprocessing/cleaning/labeling of the data done (e.g., discretization or bucketing, tokenization, part-of-speech tagging, SIFT feature extraction, removal of instances, processing

of missing values)? Yes, extensively. The full pipeline is described in Sec. 3 and comprises: (i) aesthetic and resolution pre-filtering, (ii) multi-classifier NSFW filtering and CSAM removal, (iii) intra- and inter-source URL/perceptual-hash deduplication followed by SSCD near-duplicate detection, (iv) blocked-domain and watermark filtering, (v) multi-model recaptioning with five VLMs, (vi) semantic embedding extraction (DINOv2, CLIP, SSCD), (vii) structured visual annotation (YOLO-v9e detection, YOLO-v8x classification, MediaPipe face metadata, CLIP zero-shot classification), (viii) SANA-VAE latent pre-encoding, and (ix) ethics auditing and Qwen3-VL image-style classification on a 5M and 1.5M subset, respectively.

Was the “raw” data saved in addition to the preprocessed/cleaned/labeled data (e.g., to support unanticipated future uses)? We retain the original images and original alt-text/captions alongside all derived annotations, so users can re-run alternative preprocessing or labeling pipelines. Instances removed during filtering are not redistributed; they remain available from their upstream sources via the preserved URLs.

Is the software that was used to preprocess/clean/label the data available? While the end-to-end curation code is not publicly released, the pipeline is fully described in Sec. 3 and is built almost entirely from publicly available, open-source components (e.g., YOLO-v9e/v8x, MediaPipe, DINOv2, CLIP, SSCD, SANA-VAE, and the recaptioning VLMs), enabling independent re-implementation.

Any other comments? None.

A.8.5 Uses

Has the dataset been used for any tasks already? Yes. We use MONET to pre-train a 4B-parameter text-to-image model and report downstream evaluations (FID, LongCLIP-based alignment, human studies) in Sec. 5 and the training appendix Sec. A.5

Is there a repository that links to any or all papers or systems that use the dataset? The dataset Hugging Face Hub page will link to the canonical paper and to known derivative works as they appear. Users are encouraged to cite this datasheet and notify the maintainers of derived models or datasets.

What (other) tasks could the dataset be used for? Multimodal pre-training (T2I, image-to-text VLM training, joint embedding), large-scale retrieval, near-duplicate analysis, content/style classification, dataset bias auditing. The released VAE latents specifically enable cheap latent-diffusion training without re-encoding pixels.

Is there anything about the composition of the dataset or the way it was collected and pre-processed/cleaned/labeled that might impact future uses? Yes. The Western/English-language skew (Q. Subpopulations), the imperfect recall of safety filters (Q. Offensive content), the residual noise in synthetic captions and model-inferred annotations (Q. Errors and noise) and the English-only scope all constrain downstream applicability and may propagate biases to models trained on MONET. We discuss in Sec. 6 and Sec. 7 mitigations such as rebalancing via the released ethics-audit and style annotations, output-level safety classifiers, mixing captioners at training time, and treating demographic fields as dataset-level statistics only.

Are there tasks for which the dataset should not be used? The dataset must not be used for surveillance, biometric identification, re-identification, or any application that targets individuals based on the demographic attributes annotated in the ethics audit. The model-inferred demographic fields must not be treated as ground truth or used for individual decision-making.

Any other comments? None.

A.8.6 Distribution

Will the dataset be distributed to third parties outside of the entity (e.g., company, institution, organization) on behalf of which the dataset was created? Yes; the dataset is intended for public release to the broader research community.

How will the dataset will be distributed (e.g., tarball on website, API, GitHub)? The dataset, including captions, embeddings, structured and enriched annotations, is distributed via HuggingFace <https://huggingface.co/datasets/jasperai/monet>. We also provide a FAISS-based image retrieval index within a HuggingFace space <https://huggingface.co/spaces/jasperai/monet-retrieval> in order to explore the dataset.

When will the dataset be distributed? The dataset is available now. Revisions and updates will be made available as versioned releases on the Hugging Face Hub, alongside the release of the paper.

Will the dataset be distributed under a copyright or other intellectual property (IP) license, and/or under applicable terms of use (ToU)? MONET is released under the permissive *Apache 2.0* license. All constituent real sources use commercially permissive licenses (CC-BY-4.0, MIT, or equivalent; Table 1), and the synthetic subset is generated with *Apache-2.0* models, whose outputs are redistributable. Synthetic captions and images are likewise released under *Apache 2.0*. The domain-based filters and source-governance steps applied during curation are exclusion controls, not a representation of legal clearance: users remain responsible for their own due diligence regarding the specific upstream terms applicable to their use case (Sec. 6).

Have any third parties imposed IP-based or other restrictions on the data associated with the instances? No.

Do any export controls or other regulatory restrictions apply to the dataset or to individual instances? None.

Any other comments? None.

A.8.7 Maintenance

Who will be supporting/hosting/maintaining the dataset? Jasper Research will host and maintain the dataset on the HuggingFace Hub (<https://huggingface.co/datasets/jasperai/monet>).

How can the owner/curator/manager of the dataset be contacted (e.g., email address)? The corresponding authors can be reached at `surname.name@jasper.ai` (see the title page).

Is there an erratum? Errata, if any, will be tracked on the HuggingFace dataset page and as versioned updates to the release.

Will the dataset be updated (e.g., to correct labeling errors, add new instances, delete instances)? We expect to release point updates to incorporate (i) takedown requests from depicted individuals, (ii) corrections to filters and annotations, and (iii) extensions of the ethics audit and style classification to the full pool (currently subset only; Sec. 7).

If the dataset relates to people, are there applicable limits on the retention of the data associated with the instances (e.g., were individuals in question told that their data would be retained for a fixed period of time and then deleted)? No.

Will older versions of the dataset continue to be supported/hosted/maintained? Older versions will remain accessible as Hugging Face revisions for reproducibility, but only the latest version will receive corrections and takedown updates.

If others want to extend/augment/build on/contribute to the dataset, is there a mechanism for them to do so? Yes. Contributions, additional annotations, derivative datasets and bug reports are welcomed via the Hugging Face Hub repository and the accompanying code repository. Derivative works should cite this paper and clearly document any modifications. We do not currently run a formal validation process for community contributions; significant derivative datasets that wish to be linked from the canonical Hub page will be reviewed by the maintainers before listing.

Any other comments? None.